Applied Thermal Engineering 226 (2023) 120245

Contents lists available at ScienceDirect

Applied Thermal Engineering

journal homepage: www.elsevier.com/locate/apthermeng

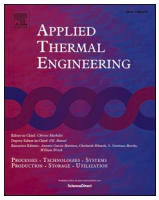

Research Paper

Comparative study of models for packed bed molten salt storage systems

Christian Odenthal [a,*], Jonas Tombrink [b], Freerk Klasing [a], Thomas Bauer [a]

[a] German Aerospace Center (DLR), Linder Höhe, 51147 Köln, Germany
[b] German Aerospace Center (DLR), Pfaffenwaldring 38-40, 70569 Stuttgart, Germany

ARTICLE INFO

Keywords:
Thermal energy storage
Model comparison
Thermocline
Packed bed
Solar thermal power

ABSTRACT

To date various models for packed bed single tank molten salt storage systems have been developed. The question arises in how far certain modelling assumptions can affect the outcome of these models. This can also depend on the applied use case, for example a short validation simulation versus an annual simulation. Thus, a comparative study is performed, considering four one-dimensional models for packed beds: the Schumann model, the continuous-solid-phase model, the single-phase model and a recently developed bidisperse model. Additionally, the impact of heat losses and variable fluid properties are considered as well. The comparison is performed for different use cases and covers the single blow operation, cyclic operation and annual simulations. Common boundary conditions are derived from a 100 MW_{el} concentrating solar thermal power plant with molten salt as heat transfer fluid. A large and a small storage volume, each with a small and a large particle packing are designed to cover a range of practical storage configurations. The aim of this work is to provide guidelines for the selection of a reasonable level of modelling detail depending on the desired accuracy and computational effort. Results indicate that the outcome can significantly differ between the use cases. Effective conductivity has visible impact in stand-by periods and small sized packings with strong thermal gradients. The single-phase model has low computing effort but is applicable only with packings in the range of millimeters. The bidisperse model has significantly improved accuracy when applied to packings with smaller particles in combination with larger particles. Heat losses showed little impact for the considered storage volumes. Temperature dependent fluid properties have an impact within short periods but average out in cyclic and annual simulations, which justifies neglecting them.

1. Introduction

Over the course of the last decades, fluid flow though packed beds have been widely investigated. Consequently, numerous publications deal with the simulation of such systems. Early publications until the 1980s were mainly driven by applications for the chemical industry [1,2] or the optimization of Cowper stoves [3,4]. In the late 1980s, the application for thermal energy storage in concentrating solar power plants emerged [5,6]. So far, the majority of publications considered a gaseous heat transfer fluid (HTF). A thorough collection of modelling approaches is described in the work by Schmidt & Willmott [7,8]. Both books describe single and two-equation modelling approaches. The authors go into detail regarding various effects such as finite conductivity on the heat transfer between fluid and solid, temperature dependent properties, several model simplifications and even some unsteady boundary conditions. However, the authors put significant emphasis into analytical solutions of the underlying equations, which are limited to constant or harmonic inflow conditions. This also restricts their comparison of some of the modelling approaches, which are eventually focused on gas flow and not liquid flow. Another comprehensive and well-known work is that of Ismail & Stuginsky [9]. The authors present several models suitable for regenerator type storage systems and undertake a parametric study for a comparison. Both water and gas flow regenerators are investigated, however, also with restrictive inflow conditions. Elouali et al. [10] published a comparative study of four models for air-based packed bed thermal energy storage (TES) in a single blow use case. Discrepancies between the investigated models were clearly visible, but it is unclear if the findings can be transferred to molten salt applications. Esence et al. [11] present a comprehensive review article about existing models and experiments regarding packed bed thermal energy storage. Focus lies on operational aspects as well as the outcome of correlations for heat transfer, conduction and pressure drop. More recently, Calderón-Vasquez et al. [12] also present a profound review on possible packed bed models for thermal energy storage with focus on heat transfer correlations, particularly on radiative heat

* Corresponding author.
E-mail address: christian.odenthal@dlr.de (C. Odenthal).

https://doi.org/10.1016/j.applthermaleng.2023.120245
Received 13 September 2022; Received in revised form 6 January 2023; Accepted 15 February 2023
Available online 21 February 2023

Nomenclature

Symbols

a_v	specific surface per volume, (m^2/m^3)
A_0	storage cross-sectional area, (m^2)
A_w	wall surface area, (m^2)
c	specific heat capacity, (J/kgK)
d_p	particle diameter, (m)
D	storage diameter, (m)
E_{stor}''	discharged exergy from storage, (J)
E_{el}	produced electricity, (J)
h	specific enthalpy, (J/kg)
h_{surf}	surface heat transfer coeff., (W/m^2K)
h_v	vol. overall heat transfer coeff., (W/m^3K)
L	storage length, (m)
$\dot{m}$	mass flow, (kg/s)
n	number of nodes, (−)
Nu	Nusselt number $d_p \cdot h_{surf}/\lambda$, (−)
p	pressure, (Pa)
P	work, (W)
Pr	Prandtl number $\mu c/\lambda$, (−)
$\dot{Q}'''$	volumetric heat source/sink, (W/m^3)
r	radial coordinate, (m)
Re	Reynolds number $v_0 d_p \rho/\mu$, (−)
s	specific entropy, (kJ/kgK)
t	time, (s)
T	temperature, (°C)
$\Delta\overline{T_f}$	mean fluid temp. diff., (K)
$\Delta T_{f,\,max}$	max. fluid temp. diff., (K)
u	specific inner energy, (J/kg)
U_w	overall wall heat transfer coeff., (W/m^2K)
V_p	particle volume, (m^3)
v_0	free flow velocity, (m/s)
w	weighting factor, (−)
x	axial coordinate, (m)

Greek symbols

Δ	difference, (−)
ε	void fraction, (−)
Θ	dimensionless temperature, (−)
λ	thermal conductivity, (W/mK)
μ	dynamic viscosity, (Pa s)
ξ	dimensionless distance, (−)
ρ	density, (kg/m^3)
τ	dimensionless time, (−)

Subscripts

a	ambient
e	end of period
eff	effective value
f	fluid
fs	fluid-solid mixture
i	node i
in	inlet
ic	inner ceiling
ig	inner ground
is	inner sections
init	initial condition
max, min	maximum, minimum
out	outlet
per	period
p, p1, p2	particle, particle 1, particle 2
PB	power block
ref	reference
s	solid
s1, s2	solid 1, solid 2
SF	solar field
stor	storage
tcd	total cycling duration
vol	volumetric
w	wall
x	position in flow direction

Superscripts

n	time step n
‘	charging period
“	discharging period

Abbreviations

HTF	heat transfer fluid
BD	bidisperse
CS	continuous-solid-phase
PDE	partial differential equation
PEC	performance evaluation criteria
SH	Schumann
SP	single-phase
TES	thermal energy storage
WL	wall loss
VP	variable fluid properties

transfer.

The application of liquids such as oil or molten salt as HTF emerged since the 2000s due to the growth of the concentrating solar power (CSP) market [13–15]. To date there are numerous publications dealing with packed bed thermocline storage systems, providing an excellent foundation for the implementation of models and supporting chosen assumptions. Several authors have implemented one or even several models for thermocline packed bed storage systems with molten salts or thermal oil [16–35]. The authors generally find a good prediction of their own or other authors experimental work with these models. A detailed overview of all mentioned publications is given in the appendix in Table 5. As shown in the following chapters several modelling assumptions differ among the authors and a systematic assessment of the impact of these assumptions is missing.

1.1. Scope of this work

Except for the work of Ismail & Stuginsky [9] and Elouali et al. [10], no comparative study suitable for packed bed molten salt thermocline storage systems has been performed so far. All other comparative studies known to the authors had their focus laid on gaseous HTFs. Therefore, it still remains unclear which modelling assumptions are of significant influence in the field of molten salt systems. For example, pressure drop and heat transfer plays an important role when gaseous HTFs are used, whilst liquid HTFs reach much better heat transfer rates and the induced pressure losses cause only small amounts of necessary pumping power. Effective conductivity is also more dominant in liquid-based systems. The shortcomings of the available literature and how they are addressed in this publication can be summarized as follows:

- As shown in Table 5 the available publications differentiate four use cases, which can be categorized in single blow (1), i.e. heating from a constant uniform temperature, additionally considered with longer stand-by periods (2). Furthermore, there is cyclic operation (3), i.e. several consecutive charging and discharging periods with constant inlet conditions and finally annual simulations (4), i.e. performing a

simulation on system level with varying inlet conditions. However, no systematic investigation of the impact of these use cases on the model outcome has been performed. For example, it is not clear whether certain differences occurring under single blow operation have an impact on annual simulations or vice versa. Therefore, all comparisons are performed under the four aforementioned use cases.

- The investigated storage volumes in the literature differ in terms of total size and packing material, which can also be deduced from Table 5. This makes it difficult to derive certain universally valid statements on the model performance. To properly investigate aforementioned models and assumptions, we firstly define a 100 MW_{el} concentrating solar power (CSP) plant as common "base case" for all simulations. Out of this, constant boundary conditions for single blow and cyclic operation are derived. For the annual simulations, a simplified power block model and solar field output data is considered. To cover a realistic range of the storage volume size, a comparatively small and a large storage volume are sized, which can provide thermal energy for the thermal power plant for 6 or 12 h, respectively. For both storage sizes, two packings, one mono-sized with small 2-mm particles and one with a bidisperse packing of 2- and 50-mm particles, are considered. With this approach a reasonable range of four possible "storage configurations" is covered.
- Finally, all publications utilize different models, which can be seen in Table 5 as well. The single-phase model (SP) assumes equal temperature of fluid and solid and therefore consists of only one partial differential equation (PDE). The Schumann model (SH) differentiates between solid and fluid and utilizes two PDEs. Moreover, the authors recently introduced a novel bidisperse model (BD), which showed differences of up to 3.5% over the SH model [36]. This model differentiates between fluid and two particle sizes and therefore includes three PDEs. The motivation for this model is that actual storage systems have differently sized rocks as filler to reduce the void fraction. Besides the three aforementioned models, there are three different effects typically considered or neglected. If effective conductivity of the bed is considered for the SH model, it is referred to as the continuous-solid-phase model (CS). Heat losses through the confining walls are taken into account with a modified version of the CS model (CS-WL). Finally, temperature dependent (variable) fluid properties are considered with a modified SH model (SH-VP). Thus, six different "models" can be compared.

From above listing, a parametric matrix of 96 configurations can be deduced. Since the BD model is not suitable for a mono-sized packing and the SP model not suitable for the bidisperse packing, the total number of possible combinations reduces to 80 variations. For a reasonable rating of the model outcome, different performance evaluation criteria (PEC) are defined, depending on the use case. Thus, this work provides a broad data set for the outcome of different modelling approaches, helping the reader to decide for the right level of detail, depending on the simulation tasks.

2. Formulation of the models

The formulation of the models contains several basic assumptions, which are discussed in the following sections.

2.1. Geometric definitions

For all simulations, the storage volume is considered as a cylindrical container, as shown in Fig. 1. The dimensions are defined by the length L and the diameter D of the storage volume. From these variables, the cross-sectional area A_0 and the area of the side walls A_w can be calculated. The container is surrounded by an insulation, which has a total heat transfer coefficient of U_w.

Filler particles for the packed bed are of irregular shape due to their natural origin. In the model it is assumed that the particles are spheres, having the same mean volume V_p as the particles. From this, the diameter d_p of the spheres is defined. In the case of bidisperse packings, two differently sized particles d_{p1} and d_{p2} exist, where d_{p1} are the larger particles. Models other than the bidisperse model consider the particle diameter as an average diameter. We use a mass weighted diameter as it reflects the thermal heat capacity of each particle. It is calculated from

$$d_p = w \cdot d_{p1} + (1 - w) \cdot d_{p2}. \tag{1}$$

Hereby, the mass fraction of the large filler is denoted by w. The void fraction is described by the variable ε and defined as the volume occupied by the fluid V_f divided by the total volume V:

$$\varepsilon = \frac{V_f}{V}. \tag{2}$$

Generally, the fluid is referred to by the subscript f and the solid filler material by the subscript s.

With these definitions, the models can be described, as follows in the next sections.

2.2. Governing equations

The modelling underlies a basic equation, which can be derived for the first law of thermodynamics [37]. It is assumed that no chemical reactions occur. The transient change in inner energy ρu equals added

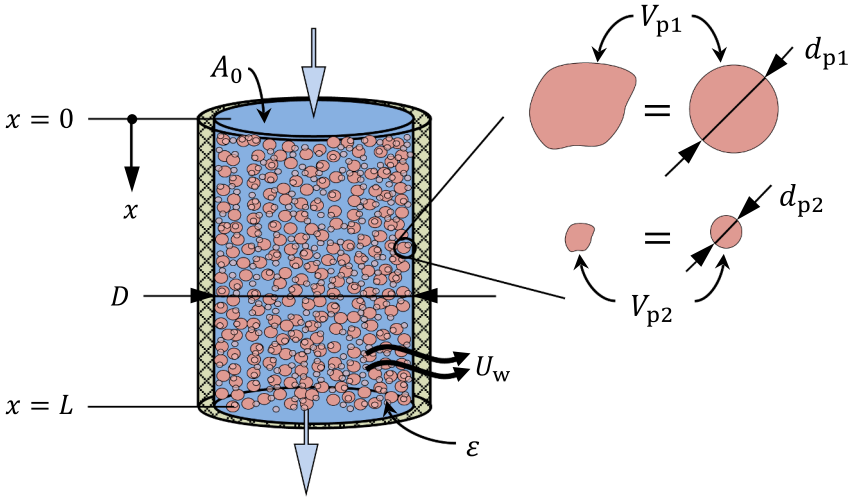

Fig. 1. Geometric properties of the storage volume and the filler particles inside.

and subtracted energy through conduction and/or convection as well as volume specific heat $\dot{Q}'''$ through heat sinks and sources:

$$\frac{\partial(\rho u)}{\partial t} = -\nabla[h\rho\vec{v} - \lambda\nabla T] + \dot{Q}'''. \tag{3}$$

Hereby, ρ denotes the density, $\vec{v}$ the velocity, λ the thermal conductivity and T is the temperature. If we assume plug flow for the fluid phase with no lateral components, i.e. $v_x \neq f(r)$, we can express above eq. (3) in a one-dimensional coordinate system with the coordinate x. With the static enthalpy $h = u + p/\rho$, the equation now reads:

$$\frac{\partial(\rho h)}{\partial t} - \frac{\partial p}{\partial t} = -\frac{\partial}{\partial x}\left[h\rho v_x - \lambda_i \frac{\partial T}{\partial x}\right] + \dot{Q}''' \tag{4}$$

For eq. (4), the following assumptions are made:

1. The fluid phase is incompressible, i.e. $\frac{\partial p}{\partial t} = 0$
2. The fluid is an ideal liquid, thus $\mathrm{d}h = c\ \mathrm{d}T$
3. Homogenous distribution of solid phases, thermophysical properties are not depending on spatial position $\lambda_x \neq f(x)$

With above assumptions and simplifications and by inserting the continuity eq. (5)

$$\frac{\partial \rho}{\partial t} + \frac{\partial}{\partial x}(\rho v_x) = 0 \tag{5}$$

into eq. (4), the basic differential equation for the model is given by eq. (6) as

$$\rho c \frac{\partial T}{\partial t} = -c\rho v_x \frac{\partial T}{\partial x} + \lambda \frac{\partial^2 T}{\partial x^2} + \dot{Q}'''. \tag{6}$$

In the next section, the different models based on this equation are described.

2.3. Description of the models

A summary of the investigated models and their characteristics is given by Table 1. All models are described and further discussed in the following sections. A detailed description of the models can be found in Ismail & Stuginsky [9], Elouali et al. [10] and Calderón-Vasquez et al. [12].

The single-phase model (SP) consists of one phase only. It requires effective conductivity, since it would otherwise reproduce a step function, resulting in numerical instabilities. Moreover, this model is only suitable for small particle sizes due to the assumption of equal temperature of both fluid and solid. The Schumann model (SH) is used as reference; it utilizes two phases and neglects effective conductivity. The impact of variable fluid properties is investigated with the Schumann model (SH-VP). Enabling effective conductivity in the Schumann model transforms it into the continuous-solid-phase model (CS). The effect of wall losses also requires effective conductivity. If effective conductivity was neglected, the heat losses would only affect the first and the last node of the computational grid. This would result in very low temperatures at only these nodes, since in that case no heat is transported from the neighboring nodes. Therefore, heat losses are considered also within the continuous-solid-phase model (CS-WL). Finally, the bidisperse model (BD) utilizes three equations without any other effects considered. This model is not appropriate for packings of particles having equal size.

2.3.1. Single-phase (SP) model

The simplest model considered in this investigation is the single-phase (SP) model. The assumption behind this model is that heat transfer between solid and fluid is very high and therefore the temperatures of the corresponding phases are equal.

This model is used in the work by Hoffman et al. [20], where three sets of experimental data are compared to the model. The model is discretized by an implicit scheme and second order accuracy both in time and space. The authors find the model faster and more accurate over a second two-equation model. Bayon et al. [28] also developed a single-phase model which is validated with several experimental data sets as well. The model is numerically solved with MATLAB's ode45 explicit solver. Results are used to derive dimensionless parameters for tank performance prediction and evaluation.

An illustration of the model and its discretization is given by Fig. 2. The storage volume is assumed to be cylindrical with cross-sectional area A_0. For the one-dimensional models, the storage volume is discretized into several layers along the flow direction with a thickness of dx. Each layer is assumed to have a uniform temperature of the fluid-solid mixture (fs).

With above assumptions, eq. (6) can be expressed for the fluid-solid mixture as

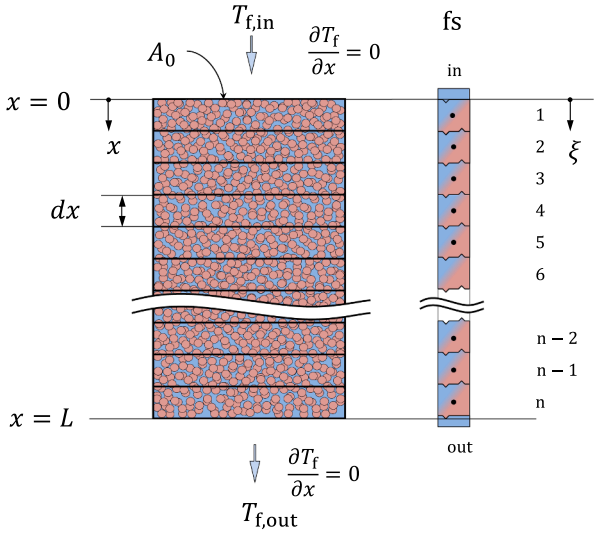

Fig. 2. Simplified representation and discretization scheme of the single-phase (SP) model.

Table 1
Summary of investigated models and their configurations.

Model	Short name	# phases	eff cond	var prop	wall loss	Equivalent model	Suitable particle sizes
Single-phase	SP	1	X				small only
Schumann (reference)	SH	2					all
Schumann with variable properties	SH-VP	2		X		= SH + var. prop	all
Continuous-solid-phase	CS	2	X			= SH + eff cond	all
Continuous-solid-phase with wall loss	CS-WL	2	X		X	= SH + eff cond + wall loss	all
Bidisperse	BD	3					small & large combined

$$\left[(1-\varepsilon)\rho_s c_s + \varepsilon\rho_f c_f\right]\frac{\partial T_{fs}}{\partial t} = -\rho_f c_f v_{0,x,f}\frac{\partial T_{fs}}{\partial x} + \lambda_{eff,x}\left(\frac{\partial^2 T_{fs}}{\partial x^2}\right). \quad (7)$$

The transient term contains the mean heat capacity of the fluid and solid mixture, where ε is the void fraction of the solid, ρc the volumetric heat capacity of the fluid or solid, respectively, $v_{0,\,x,\,f}$ is the free flow velocity of the fluid. Conduction of the fluid and solid mixture is considered by the effective conductivity $\lambda_{eff,\,x}$ as defined by eq. (16) in section 2.3.4.

2.3.2. Schumann (SH) and continuous-solid-phase (CS) model

A more realistic model is the continuous-solid-phase (CS) model, which uses two coupled partial differential equations for the solid and fluid. If no effective thermal conductivity of the bed is used, this model is often referred to as the Schumann (SH) model [38], developed in 1929. An illustration of the model is shown in Fig. 3. Outer dimensions and discretization are similar to the single-phase model in the preceding section.

The Schumann model is used by van Lew et al. [22] to implement a model which uses the trapezoidal rule for discretization. Investigations with the model are based on purely non-dimensional calculations. The model is later used by Li et al. [23] and Reddy et al. [24] for further investigations. Valmiki et al. [21] also use the Schumann model which is validated with data of an experiment with rapseed oil. No further information about the numerical procedure is given.

The continuous-solid-phase (CS) model is used by most authors. Hoffmann et al. [20] use this model alongside their single-phase model for a comparison. The numerical solution is also achieved by an implicit second order discretization. The authors find higher accuracy over the single-phase model, particularly in small-size tanks. Flückiger et al. [30] discretize their model with a first order implicit and second order spatial discretization. They use a quadratic flux limiter for the convective terms to improve accuracy. They use their model for system level simulations. Yang et al. [31] also use implicit transient discretization and investigate specific performance criteria for a fictive storage material. Niedermeier et al. [34] use a second order Crank-Nicholson scheme for the transient discretization and first order upwind and central differences for the spatial discretization. They compare the performance of a molten salt packed bed to a pure sodium packed bed. Others utilize a 2D CS model. Yang and Garimella [17,18] use FLUENT to set up such model, which is also used by Flückiger et al. [19]. Consequently, the flow pattern is also simulated instead of assuming plug flow. Yin et al. [29] chose the same approach by using FLUENT. They investigate a system of molten salt and SiC balls. Xu et al. [32] developed their finite volume own code for solving the 2D-CS model. They investigate a Solar Salt and quartzite rock. Finally, Votyakov et al. [26] developed a model using an analytical solution which is later used by Bonanos et al. [27] for a comprehensive parametric study for tank design. Kocak and Paksoy [35] use both SH und CS model and compare the prediction of an oil-based pebble bed TES system. They find little deviation between temperature curves and a reduction in charging time of approx. 4 min with the CS model compared to the SH model.

It is possible to further improve the CS model by discretizing the temperature profile inside the particles, instead of assuming uniform particle temperature. This model is referred to as the dispersion-concentric (DC) model. The model is not considered here, but a description is given by Ismail & Stuginsky [9] and Elouali et al. [10]. Further literature can be found by Zhao et al. [16], Galione et al. [25] or Xu et al. [33].

In the CS model, the equation for the fluid is similar to that of the single-phase model. The transient term now contains only the thermal capacity of the fluid instead of both solid and fluid. An additional term $\dot{Q}'''_{f-s}$ accounts for the heat transfer between fluid and solid (s1), see eq. (12). If heat transfer to the ambient $\dot{Q}'''_{f-a}$ is also considered (see eq. (17)), it is associated to the fluid side.

$$\varepsilon\,\rho_f\,c_f\frac{\partial T_f}{\partial t} = -\rho_f\,c_f\,v_{0,x,f}\,\frac{\partial T_f}{\partial x} + \underbrace{\lambda_{eff,x}\left(\frac{\partial^2 T_f}{\partial x^2}\right)}_{\text{CS model only}} + \dot{Q}'''_{f-s} + \dot{Q}'''_{f-a} \quad (8)$$

The second partial differential equation accounts for the solid side. The transient term on the left-hand side contains the thermal capacity of the solid which is coupled to the fluid equation by the source term $\dot{Q}'''_{f-s}$ (eq. (12)).

$$(1-\varepsilon)\rho_s c_s\frac{\partial T_s}{\partial t} = -\dot{Q}'''_{s-f} \quad (9)$$

2.3.3. Bidisperse (BD) model

The Schumann model assumes a uniform temperature as well as a uniform size for all solid particles. If the particle sizes significantly differ, using a mean diameter for all particles may result in inaccurate results.

The bidisperse model is based on the Schumann model except for the difference that two partial differential equations are used for the solid particles, see Fig. 4. The equations are referred to by the subscripts (s1) and (s2). For the particle diameter of each of the two solid equations a suitable mean value must be considered. The equation for the fluid now

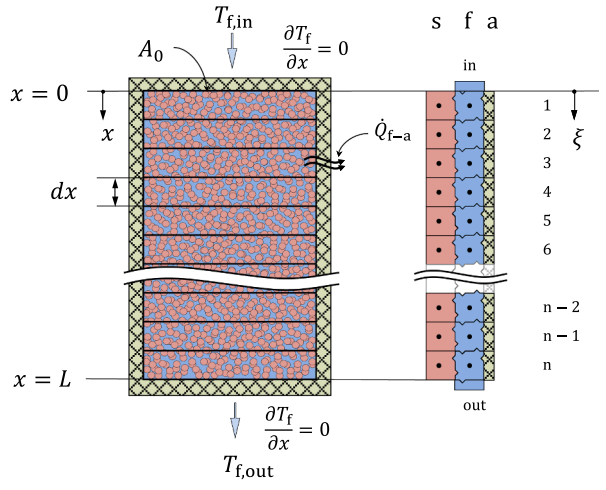

Fig. 3. Simplified representation and discretization scheme of the continuous-solid-phase model.

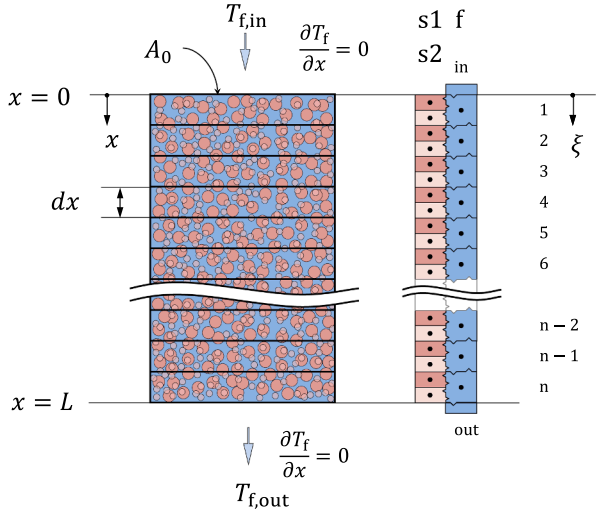

Fig. 4. Simplified representation and discretization scheme of the bidisperse model.

has two source terms, $\dot{Q}'''_{f-s1}$ and $\dot{Q}'''_{f-s2}$, coupling the fluid with the two solid phases:

$$\varepsilon\rho_f c_f \frac{\partial T_f}{\partial t} = -\rho_f c_f v_{0,x,f}\frac{\partial T_f}{\partial x} + \dot{Q}'''_{f-s1} + \dot{Q}'''_{f-s2}. \quad (10)$$

For the solid, the two equations read

$$w\cdot(1-\varepsilon)\rho_{s1}c_{s1}\frac{\partial T_{s1}}{\partial t} = -\dot{Q}'''_{f-s1} \text{ and}$$

$$(1-w)\cdot(1-\varepsilon)\rho_{s2}c_{s2}\frac{\partial T_{s2}}{\partial t} = -\dot{Q}'''_{f-s2} \quad (11)$$

Contrary to eq. (9), a weighting factor w with $0 < w < 1$ is introduced, which describes the share of the solid *s*1 on the total amount of solid. We assume equal density $\rho_{s1} = \rho_{s2} = \rho_s$ and thus equal volume and weight ratio. The temperatures and the lumped heat transfer coefficient must be considered for both solid phases s1 and s2. Further details are given in section 2.3.4.

2.3.4. Common physical values and correlations

2.3.4.1. Source terms and lumped volumetric heat transfer coefficient. The source terms are used in the Schumann (SH), continuous-solid-phase (CS) and bidisperse (BD) models. The source term coupling eq. (8) and (9) in the SH/CS model is calculated from

$$\dot{Q}'''_{f-s} = h_v\cdot(T_s - T_f). \quad (12)$$

In case of the bidisperse model, two different source terms $\dot{Q}'''_{f-s1}$ and $\dot{Q}'''_{f-s2}$ must be calculated for the solids (s1) and (s2), where h_v and T_s must be distinguished.

The lumped volumetric heat transfer coefficient h_v is calculated from eq. (13). This equation consists of the surface film coefficient h_{surf} and a second term for the thermal resistance through conduction [7].

$$h_v = a_v\cdot\left(\frac{1}{h_{surf}} + \frac{5\cdot d_p}{2\cdot\lambda_s}\right)^{-1} \quad (13)$$

For the bidisperse model d_p and λ_s must be distinguished, thus two different a_v and h_{surf} must be calculated.

The specific surface per volume a_v is calculated from the void fraction ε. For the bidisperse model $a_{v,\,1}$ and $a_{v,\,2}$ must be calculated by adding the weighting factor *w*. The equations thus read as followed:

$$a_v = \frac{6(1-\varepsilon)}{d_p}, a_{v,1} = w\frac{6(1-\varepsilon)}{d_{p1}}, a_{v,2} = (1-w)\frac{6(1-\varepsilon)}{d_{p2}}. \quad (14)$$

The surface film heat transfer coefficient h_{surf} is calculated by a widely used formula presented by Wakao et al. [39], where *Pr* is the Prandtl number and *Re* the particle Reynolds number:

$$Nu = \frac{d_p h_{surf}}{\lambda_s} = 2 + 1.1\cdot Pr^{1/3}\cdot Re^{0.6}. \quad (15)$$

To distinguish h_{surf} for the bidisperse model, d_p, λ_s and *Re* must be calculated for both particle sizes.

2.3.4.2. Effective thermal conductivity of the bed. Effective thermal conductivity is used in the single-phase (SP) and the continuous-solid-phase model (CS & CS-WL). A common approach for modelling the thermal conductivity of the bed is using an effective thermal conductivity λ_{eff} which is then considered in the fluid term of the equations. Several modelling approaches exist, whereby some are very sophisticated as summarized by Esence et al. [11]. Wakao et al. [39] also consider an additional turbulent term in eq. (16), which accounts for turbulent mixing. As stated by Balakrishnan and Pei [2], turbulent mixing is already incorporated in fully empirical heat transfer correlations. Thus, the effect would occur twice in the convective and conductive terms of the fluid PDE, exaggerating the thermal destratification.

The approach chosen in this work assumes that thermal resistance is a series arrangement of the thermal resistances of solid and fluid, weighted by the void fraction ε of the bed [40]. This is also the most common approach in the literature. The effective thermal conductivity in flow direction $\lambda_{eff,x}$ is then expressed by

$$\lambda_{eff,x} = \left(\frac{1-\varepsilon}{\lambda_s} + \frac{\varepsilon}{\lambda_f}\right)^{-1}. \quad (16)$$

Hereby, λ_s is the thermal conductivity of the solid and λ_f of the fluid, respectively.

2.3.4.3. Thermophysical properties. Correlations for thermophysical properties of Solar Salt are taken from Bauer et al. [41]. Those for basalt rocks were correlated by own fits to the data given by Hartlieb et al. [42]. Polynomic coefficients for the correlations are summarized in Table 2.

2.3.5. Description of additional considered effects

The following chapter describes the two assumptions and simplifications implemented in the prescribed models.

2.3.5.1. Variable thermophysical properties (-VP). To consider the temperature dependency of the variable thermophysical properties, various approaches exist. A common approach is point iteration where the new temperature profile and thermophysical properties are repeatedly calculated at the new time step until the residuum between the last calculations reaches a certain threshold. A significantly faster method is the previous time step approximation, where thermophysical properties are calculated from the temperatures of the preceding time step without any iteration. In the present case, this approximation would be justified, since time steps are comparatively small and temperature changes are very low between time steps.

Since it is still necessary to calculate several thermophysical properties at each node, a linear interpolation as further simplification and acceleration of the computing time is used. This is achieved by calculating the matrix coefficients at three different temperatures and three mass flow rates (minimum, mean and maximum). All matrix coefficients are then calculated by a fast linear interpolation. The model used for the comparison is the Schumann model, thus the variable fluid properties model is referenced as SH-VP.

2.3.5.2. Wall losses (-WL). The source term considering heat losses to

Table 2
Correlations used for the calculation of temperature dependent thermophysical properties.

Property		b*T^3	c*T^2	d*T	e
Solar Salt [41]	c_f			$3.092 \bullet 10^{-2}$	$1.540 \bullet 10^{+3}$
	λ_f			$3.452 \bullet 10^{-4}$	$3.804 \bullet 10^{-1}$
	ρ_f			$-6.697 \bullet 10^{-1}$	$2.106 \bullet 10^{+3}$
Basalt [42]	c_s	$7.137 \bullet 10^{-7}$	$-1.490 \bullet 10^{-3}$	1.193	$7.464 \bullet 10^{+2}$
	λ_s	$7.859 \bullet 10^{-10}$	$-1.495 \bullet 10^{-6}$	$6.038 \bullet 10^{-4}$	1.553
	ρ_s				$2.992 \bullet 10^{+3}$

the ambient $\dot{Q}''_{f-a}$ is given by eq. (17). It uses a total heat transfer coefficient $U_{w,is}$ for the heat transfer through the inner side walls of the storage tank. For the ceiling and the ground section, additional total heat transfer coefficients $U_{w,ic}$ and $U_{w,ig}$, respectively, are considered.

$$\dot{Q}''_{f-a} = (T_a - T_f)\cdot\frac{1}{A_0\cdot L}\left[A_{w,is}\cdot U_{w,is} + \begin{cases} \frac{L}{dx}\cdot A_0\cdot U_{w,ic} & \text{ceiling section} \\ 0 & \text{inner sections} \\ \frac{L}{dx}\cdot A_0\cdot U_{w,ig} & \text{ground section} \end{cases}\right] \tag{17}$$

Wall losses are investigated alongside the continuous-solid-phase model, thus, the model with wall losses is referenced as CS-WL.

2.4. Implementation

2.4.1. Removal of dimensions

The dimensions of the equations are removed according to eq. (18). We use a fixed reference value T_{ref} and t_{ref}, for the temperatures and time, respectively. The dimension of length is removed by dividing through the length of the storage volume.

$$\Theta = \frac{T}{T_{ref}},\quad \tau = \frac{t}{t_{ref}},\quad \xi = \frac{x}{L}. \tag{18}$$

2.4.2. Discretization of the equations

Transient discretization is done by a fully implicit scheme. At node i, the derivative with respect to time reads

$$\frac{\partial\Theta}{\partial\tau} = \frac{\Theta_i^{n+1} - \Theta_i^n}{\Delta\tau}. \tag{19}$$

The convective derivative is discretized by a second order upwind scheme, which is

$$\frac{\partial\Theta}{\partial\xi} = \frac{\Theta_{i-2}^{n+1} - 4\Theta_{i-1}^{n+1} + 3\Theta_i^{n+1}}{2\Delta\xi}. \tag{20}$$

For conductive terms, central differences are taken. This is a second order accurate scheme:

$$\frac{\partial^2\Theta}{\partial\xi^2} = \frac{\Theta_{i+1}^{n+1} - 2\Theta_i^{n+1} - \Theta_{i-1}^{n+1}}{\Delta\xi^2}. \tag{21}$$

2.4.3. Boundary and initial conditions

The boundary conditions of the PDEs must only be considered for the fluid temperatures and can be described as followed. In the inlet region, fluid temperatures at nodes outside the domain have a constant value of $\Theta_{f,in}$

$$\xi = 0: \quad \Theta_{f,-2} = \Theta_{f,-1} = \Theta_{f,in}. \tag{22}$$

In the outlet region, it is assumed that no heat flux is occurring, hence the outlet condition reads

$$\xi = 1: \quad \frac{\partial\Theta_f}{\partial\xi} = 0. \tag{23}$$

The models consider a constant mass flow inside the storage volume, thus

$$\xi = 0\ldots1: \quad \dot{m}_i = \dot{m}_{f,in} \Leftrightarrow v_{i,x} = \frac{\rho_i A_0}{\dot{m}_{f,in}}. \tag{24}$$

Initial conditions at $\tau = 0$ and nodes i are set up for both fluid and solid, according to

$$\tau = 0: \quad \Theta_{f,i} = \Theta_{s,i} = \Theta_{init}. \tag{25}$$

2.4.4. Implementation and validation in MATLAB

By inserting above equations into the PDEs of the different models, one yields a set of ordinary differential equations (ODEs), which leads to a system of linear dependent equations. They can be described by

$$\left(\bar{\bar{I}} + \bar{\bar{M}}^{n+1}\right)\cdot\boldsymbol{\Theta}^{n+1} = \boldsymbol{\Theta}^n + \boldsymbol{b}. \tag{26}$$

Hereby, $\bar{\bar{I}}$ is the identity matrix, $\bar{\bar{M}}^{n+1}$ a sparse band matrix, $\boldsymbol{\Theta}^{n+1}$ and $\boldsymbol{\Theta}^n$ the vectors of the temperature field for the next and current time step, whilst vector $\boldsymbol{b}$ contains the boundary conditions. The linear system is solved by the Matlab® routine mldivide.

The bidisperse and Schumann model have been validated in a previous publication by the authors [36]. As a validation section would add substantial depiction to the present work we would like to reference aforementioned publication at this point.

3. Investigated use cases and methodology for comparison

In this chapter the considered use cases are described and which boundary conditions as well as storage dimensions can be derived from these. To allow a comparison of the results, the performance evaluation criteria (PEC) and methodology are described.

3.1. Common base case of for the investigations

Since thermal energy storage has a wide field of applications, a first step is the definition of an application, from where temperature level and thermal power can be derived. For convenience, the resulting parameters are slightly rounded. In this work, a packed bed thermocline thermal energy storage system with Solar Salt as HTF and basalt rock as filler is assumed. This TES system is integrated in a solar thermal power plant. A simplified scheme for the plant has been developed by the authors beforehand [43] (see also section 3.2, Fig. 5). The plant has an electrical power output of 100 MW_{el}, which translates into a nominal thermal power of 235 MW_{th}. The inlet temperature of the power block is 550°C and the outlet temperature 312 °C. Rounding the outlet

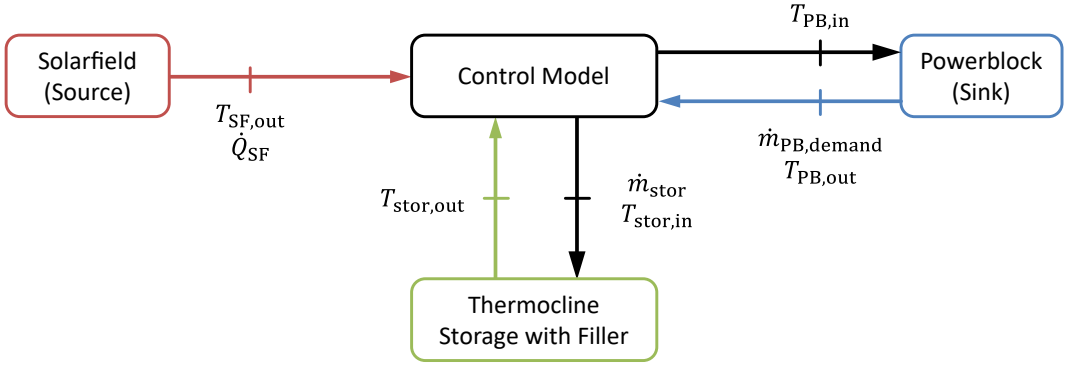

Fig. 5. Working principle of the model for annual simulation.

Table 3
Overview of all studies, boundary conditions and performance evaluation criteria (PEC).

Study	Inlet conditions	Performance evaluation criteria (PEC)	Visualization
Grid study	$T_{f,\,in} = 550\ ^\circ C$ $\dot{m}_{f,in} = 630\ kg/s$	Temperature differences $\Delta\overline{T_f}$ (mean) and $\Delta T_{f,max}$ (max), execution time Δt_{exec}	Temperature profiles
Single blow and hold	$T_{f,\,in} = 550\ ^\circ C$ $\dot{m}_{f,in} = 630\ kg/s$	Temperature differences $\Delta\overline{T_f}$ (mean) and $\Delta T_{f,max}$ (max)	Temperature profiles after single blow and after hold
Cyclic operation	$T_{f,\,in} = 550/310\ ^\circ C$ $\dot{m}_{f,in} = 630\ kg/s$	Time differences charging / discharging $\Delta t_{per}'$ and $\Delta t_{per}''$, total cycling duration Δt_{tcd}	Temperature profiles at beginning of last discharge cycle
Annual simulation	$T_{f,\,in} = var$ $\dot{m}_{f,in} = var$	Produced electricity ΔE_{el}, discharged exergy $\Delta E_{stor}''$	Full load hours each day

temperature to 310°C and using the formula given in Table 2, to calculate the heat capacity, the necessary mass flow rate of Solar Salt can be derived, which is 630 kg/s. To account for the heat losses, some simplifications are made. Losses through the walls and the ground are treated equally. The total heat transfer coefficient is estimated to 0.2 W/m^{2}K and the ambient and ground temperatures are assumed constant at 20 °C. The common boundary conditions are summarized in the first part of Table 6.

3.2. Use cases and performance evaluation criteria

The models are compared with different inlet boundary conditions within the three different use cases. Different performance evaluation criteria (PEC) are defined in the following subsections for these operation modes and PEC are summarized in Table 3.

3.2.1. Single blow and hold

In the single blow operation, the storage volume is charged or discharged at constant inlet conditions, starting from a uniform initial temperature of filler and molten salt. This case causes the strongest gradients and also eliminates many outer influences. The influence of intra-particle conduction can be assessed, when the mass flow through the storage volume is set to zero.

For the present simulations, the storage volume is charged with a step function for mass flow from zero to the nominal value for the duration of half of the design storage time. Here, the mass flow is set with a step function to zero again. Subsequently, the simulation continues for another 24 h to assess the intra-particle conduction.

To assess the performance, the mean temperature difference $\Delta\overline{T_f}$ at the end of the storage operation is calculated between the temperature curve of the considered model and the temperature curve of the Schumann model, which acts as reference. To calculate $\Delta\overline{T_f}$, the absolute differences at each fluid node i are taken.

$$\Delta\overline{T_f} = \frac{1}{n}\sum_i \left| T_{f,i} - T_{f,i}^{SH} \right| \tag{27}$$

Furthermore, the maximum occurring temperature difference $\Delta T_{f,max}$ between the Schumann and the current model is calculated from

$$\Delta T_{f,max} = max\left| T_{f,i} - T_{f,i}^{SH} \right|. \tag{28}$$

For the grid study, which is performed with the single blow operation, we also compare the execution time of the model Δt_{exec}. All calculations are performed on an Intel Xeon CPU E5–1660 v4 @ 3.20GHz.

3.2.2. Cyclic operation

The cyclic operation allows investigating the development of a thermocline zone. This is of particular interest when the allowed change of the exit temperature is comparatively small. This leads to a broad thermocline which needs up to several dozens of cycles before a quasi-stationary state is reached. In this case of application, developments of the thermocline zone become visible, which are barely notable in the single blow operation.

For the cyclic operation, temperature differences would not be expedient, since the positions of the temperature curves differ as well. Instead, the total time for the last charging and discharging periods $\Delta t_{per}'$ and $\Delta t_{per}''$ as well as the total cycling duration Δt_{tcd} are compared to the Schumann model (SH). This approach allows a better comparison to clarify differences of the model outcome in the long term.

3.2.3. Annual simulation

For the annual simulation, the storage model is coupled with a heat source and a heat sink. All three components (storage, source and sink) are controlled by a control model. The working principle is illustrated by Fig. 5.

As source, a solarfield is considered. The solarfield is a time series of thermal power output, which has been derived from a Greenius model [44]. The source data has a time step length of 10 min, which is linearly interpolated by the model to a step size of one second. It is assumed, that the solarfield supplies a constant outlet temperature of 550°C. The control model calculates the inlet temperature into the source. This can be a mixing temperature if power block and storage are running simultaneously or just the return temperature from one of the two. From these variables, the mass flow through the source is calculated, but limited to a maximum of 1500 kg/s. If the limit is reached, it is assumed that excess energy is avoided by defocusing the solar field.

As sink, a simplified power block model is considered. The model has been developed in EBSILON Professional, which was subsequently parameterized in a previous study by the authors. The control model attempts to supply the sink first. To do so, the mass flow demand of the sink for a given inlet temperature is requested from the sink model. The sink model returns the necessary mass flow for maximum power output. If the mass flow supply by the source is sufficient, the model outputs the outlet temperature and the electric power generation.

Any solar excess mass flow is diverted to the storage volume. If the supplied mass flow falls below the demand, the storage volume is used to keep the power block running at full load, but only if there is a minimum amount of 235 MWh of energy already stored. Another exception is when the storage contains <235 MWh of energy and the sink is not operational, which usually happens at the beginning of a new day. In this case, the control model supplies energy to the storage first.

For the annual simulation, calculating the temperature deviations are not reasonable since they reflect only the impact of the last cycles. Instead, a cumulative value is more expedient. For the present study, the total exergy E_{stor}'' provided by the storage system during the discharging periods is compared. This is a direct measure of the storage output and thus a reasonable evaluation criterion for the storage model performance. The exergy of the k^{th} discharge period during $t_{0,k}''$ to $t_{e,k}''$ is calculated according to eq. (29). Here, $\dot{m}_{HTF}$ is the HTF mass flow, $T_{out}''(t)$ the exit temperature, T_a the ambient temperature in Kelvin and h and s are the specific enthalpy and entropy, respectively.

$$E_{stor}'' = \sum_k \int_{t_{0,k}''}^{t_{e,k}''} \dot{m}_{HTF} \cdot \left[h\left(T_{out}''(t)\right) - h(25^\circ C) - T_a \cdot \left(s\left(T_{out}''(t)\right) - s(25^\circ C) \right) \right] dt_k \tag{29}$$

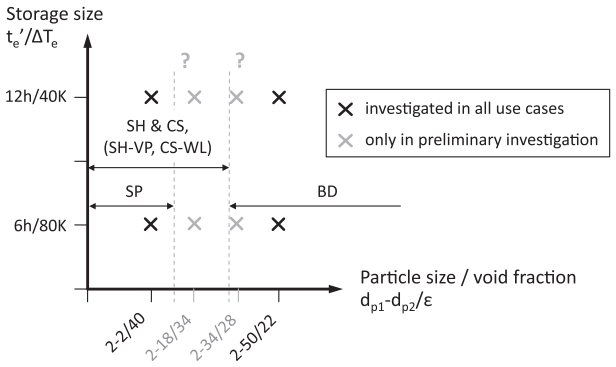

Fig. 6. Overview of investigated storage configurations and suitable models for the investigation.

Furthermore, the produced electric energy E_{el} is also compared. The produced electric energy is calculated from the integral over the total cycling duration of electricity output of the sink model:

$$E_{el} = \int_0^{t_{tcd}} P_{el,out}(t)\, dt_{tcd}. \tag{30}$$

As performance evaluation criteria (PEC), the differences to the Schumann model are calculated. Thus, the PECs are

$$\Delta E_{el} = E_{el} - E_{el}^{SH} \text{ and } \Delta E_{stor}^{''} = E_{stor}^{''} - E_{stor}^{''SH}. \tag{31}$$

It should be noted, that a significant fraction of the electric energy is produced directly from heat of the solar field. Hence, compared to the exergy output of the storage E_{stor}'', the differences to the Schumann model are expected to be barely half.

3.3. Definition of storage volume and packing dimensions

The simulations should cover a representative range of storage volumes. However, the variation of only some parameters would quickly potentiate into a huge parameter set. Therefore, it is necessary to define a parameter set by some practical considerations.

Size of the storage volume: The first aspect to consider is the dimension of the storage volume. The capacity and thus size of the storage volume is mainly affected by thermal power and storage time. Since thermal power is fixed by the system boundary conditions, the storage time is one of the variable parameters. The storage time considered here is the time for charging the storage volume t_e' after reaching cyclic steady state, i.e. when the time difference between two consecutive charging cycles is not changing any more. The storage volume is considered as "full", when a certain permitted change of the exit temperature ΔT_e is reached. The permitted change of the exit temperature also affects the storage size, because it affects the thickness of the thermocline region. The thermocline is expanding from the beginning of the first cycle due to heat conduction and limited heat transfer between fluid and solid. In the moment of switching from charging to discharging, or vice versa, larger temperature differences occur, which is narrowing the thermocline in this area. With increasing permitted change in exit temperature for the preceding cycle, those temperature differences increase and the thermocline region becomes smaller. In the present work, we want to consider a "large" storage volume, where we assume 12 h of operation and a ΔT_e of 40 K. As counterpart, the "small" storage volume has 6 h of storage time and a higher ΔT_e of 80 K. Both sizes are shown in Fig. 6.

Particle dimensions: The second aspect to consider is the size and void fraction of the filler material. Bearing in mind the assumptions behind the different models, it is evident that not all models are suitable for all filler sizes. The assumption of the single-phase model (SP) of uniform temperature between solid and fluid is only valid when heat transfer is infinite as in the case of infinitely small particles. Hence, there must be a certain particle size, where the outcome of the SP model can be considered barely precise enough. On the other end of the spectrum, the bidisperse model (BD) is only reasonable, when the difference of both particle sizes is large enough. Towards smaller particles it will be sufficient to consider an average particle diameter with either the Schumann (SH) or the continuous-solid-phase (CS) model. The useful ranges of the models are also indicated in Fig. 6. The void fraction of the packing material can be linked to the particle size by practical considerations. A mixing of the 2-mm particles with even smaller ones would not be feasible. Hence, the "small" particle size packing is assumed as a mono-sized packing of 2-mm particles. In this case, the void fractions are reported to be around 40% [20]. On the other end of the spectrum, we assume large particles with a diameter of 50 mm. Since purpose of thermocline storage with filler is reducing the void fraction, a mono-sized packing is not useful, since the void fraction would not reduce. By filling the voids of the larger packing by small particles, the resulting void fractions are reported to be around 22% [13,45]. A typical size ratio large to small would be 70 to 30 [46]. Hence, the "large particle size packing" is considered as a mixture of 50-mm (70%) and 2-mm (30%) particles. The resulting parameter set is illustrated in Fig. 6, marked by the four black crosses.

With above gradations of storage size and particle dimensions, four storage configurations are covered. For a better understanding of suitable ranges, particularly for the SP and BD models, two additional size ratios 2–18 and 2–34 are considered. It is assumed that the void fraction is changing linearly from 40% to 22%. These intermediate size ratios are also illustrated in Fig. 6 by grey crosses. These intermediate size ratios will be considered in a preliminary investigation in the next chapter. All data is also summarized in the second section in Table 6.

3.4. Criterions for the model comparison

As stated beforehand, the Schumann model (SH) is used as reference for model comparison (see section 3.2). That means all utilized

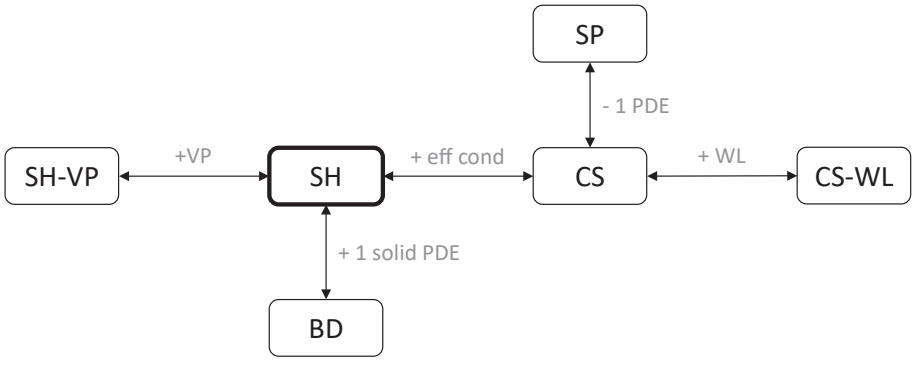

Fig. 7. Simplified scheme for the comparison of the models to each other.

performance evaluation criteria (PEC) are in relation to the SH model. Since BD, CS and SH-VP distinguish themselves from the SH model only in terms of one criterion (third partial differential equation (PDE), effective conductivity or variable fluid properties (VP), respectively), these models can directly be compared to the SH model, see Fig. 7.

The single-phase model (SP), however, has two distinctions from the SH models, namely effective conductivity and the reduction to one PDE. Thus, if we want to assess the impact of the reduction to one PDE, we need to exclude the impact of effective conductivity. Thus, one needs to compare the SP model to the CS model (see Fig. 7). The effect of wall losses (-WL) requires also effective conductivity (eff cond) to be present (see section 2.3). Therefore, the impact of wall losses becomes apparent only when comparing the CS-WL model to the CS model (see Fig. 7).

4. Results

In this chapter results are presented. First, some preliminary investigations are carried out to determine store size, grid size, time step and suitability of the models regarding different particle dimensions. Then results of the three use cases are presented. These are single blow and hold, storage operation with constant charge/discharge cycles, integration of storage in a CSP plant with annual simulation. Within each section between mono- and bi-disperse packing is distinguished.

4.1. Preliminary investigations to determine storage and grid size

In this chapter preceding simulations are performed. The first section covers sizing calculations of the storage volume. The following sections cover a grid study for spatial and temporal resolution and a short investigation of suitable packing size ranges of the different models.

4.1.1. Sizing procedure of the storage volume

Typical values for two-tank storage systems are in the range of 12–14 m [47]. For simplification, the length (i.e. height) of the storage volume is assumed to be 10 m in this study. As particle diameter, the respective mean value is considered. Alongside the previously defined assumptions and specifications, the storage diameter can thus be determined. The Schumann (SH) model is used to calculate repeated charging and discharging cycles until cyclic steady state is reached, i.e. the duration of the last two consecutive charging or discharging periods does not change more than one time-step. A simplex algorithm is used to adjust the cross-sectional area in a way, that the predefined charging time of 12 or 6 h, respectively, is reached. The resulting dimensions are summarized in the last section of Table 6.

For the preliminary investigation of the intermediate particle sizes, mean values for the storage diameter are used. These are 720 m^2 for the 6 h/80 K-configuration and 1700 m^2 for the 12 h/40 K-configuration.

4.1.2. Grid study

Through the spatial discretization, terms of order $\mathscr{O}(\Delta x^3)$ and higher are neglected which introduces a slight error. This is causing an artificial diffusion, often referred to as numerical diffusion, which can be minimized by a high spatial discretization. Thus, it is mandatory having an estimate for the amount of diffusion and this is subsequently presented.

For a grid study, simulations with the larger 2–50/0.22 and the smaller 2–2/0.40 particles must be distinguished. The smaller particles cause stronger gradients demanding smaller grid sizes and time steps which eventually results in a longer computing time. If larger particles are considered, gradients are much weaker. Thus, the Schumann (SH) and single-phase (SP) models are used. Since the impact of the small particles in the bidisperse model is unclear, the BD model is also briefly considered. Simulations are run with the 6 h/80 K storage configurations, since the thermal gradient is generally highest here. The mean temperature difference $\Delta\overline{T_f}$, the maximum temperature difference $\Delta T_{f,max}$ and the computing time Δt_{exec} are summarized in Table 4.

4.1.3. Variation of time step length

Fig. 8 shows the temperature profiles after 3 h charging (single blow), starting from the initial temperature for the SH and SP model. A

Table 4
Summary of grid study results; mean and maximum temperature differences and execution time for a variation of time step and grid size; investigated models are Schumann (SH), single-phase (SP) and bidisperse (BD).

Model	SH			SP			BD		
Variation of time step									
Grid size:	**dx = 0.05 cm**			**dx = 0.05 cm**			**dx = 0.05 cm**		
dt / s	$\Delta\overline{T_f}$ / K	$\Delta T_{f,max}$ / K	Δt_{exec} / s	$\Delta\overline{T_f}$ / K	$\Delta T_{f,max}$ / K	Δt_{exec} / s	$\Delta\overline{T_f}$ / K	$\Delta T_{f,max}$ / K	Δt_{exec} / s
0.02	–	–	7901.6	–	–	5005.0	–	–	30292.0
0.05	0.00	0.00	3342.1	7.24	11.96	2001.6	0.00	0.00	13908.2
0.1	0.00	0.01	1636.7	16.76	25.37	983.4	0.00	0.01	7120.4
* ***0.2***	0.01	0.02	802.6	***29.43***	***40.58***	***506.0***	0.01	0.01	3596.2
† ***0.5***	0.03	0.05	321.9	***47.06***	***59.69***	***198.3***	0.02	0.04	1410.9
1.0	0.06	0.10	179.3	58.23	72.15	101.2	0.04	0.07	699.4
‡ ***2.0***	***0.11***	***0.20***	***89.2***	66.87	82.69	51.5	***0.08***	***0.15***	***348.7***
5.0	0.29	0.49	36.1	74.99	93.86	21.2	0.21	0.36	136.6
Variation of grid size									
Time step:	**dt = 2.0 s**			**dt = 0.2 s**			**dt = 2.0 s**		
dx / cm	$\Delta\overline{T_f}$ / K	$\Delta T_{f,max}$ / K	Δt_{exec} / s	$\Delta\overline{T_f}$ / K	$\Delta T_{f,max}$ / K	Δt_{exec} / s	$\Delta\overline{T_f}$ / K	$\Delta T_{f,max}$ / K	Δt_{exec} / s
* **0.05**	–	–	90.0	**–**	**–**	**490.1**	–	–	362.6
0.1	0.00	0.01	38.0	3.09	8.59	245.0	0.00	0.01	172.1
† ***0.2***	0.01	0.02	17.0	***8.78***	***20.48***	***135.6***	0.01	0.02	83.0
0.5	0.04	0.06	7.1	19.53	30.34	56.1	0.04	0.05	31.7
1.0	0.08	0.12	3.8	28.39	39.17	34.5	0.08	0.11	15.1
‡ ***2.0***	***0.18***	***0.29***	***2.6***	36.30	50.95	21.8	***0.16***	***0.26***	***7.2***
5.0	0.69	1.11	1.5	44.40	64.02	15.6	0.54	0.90	3.8
10.0	2.22	3.68	1.3	48.96	71.43	13.7	1.68	2.63	2.6

Selected time step and grid size:
* for 2–2/0.40 packing with single blow / cyclic simulations
† for 2–2/0.40 packing with annual simulations
‡ for 2–50/0.22 packing with all simulations.

Table 5
Overview of numerical models for thermocline storage with molten salt or thermal oil as HTF.

[1]Publication	Material fluid solid	Particles d[mm] / eps[−]	Temp. [°C] low / high	Size mass flow	Storage volume height [m] / diameter [m]	Operation	Model flow [2]discretization	Eff cond	Heat loss	[3]Grid size time step	Variable properties	[4]Numerical solution
Zhao et al. (2017) [16]	Solarsalt quartzite & sand PCM capsules	19.05 / 0.22 10 / 0.34	288 / 570	250 MW -	14 / 30.4–44.4	cyclic	1D-DC plug flow	static & dynamic fluid	no	200n 10s	yes, iterative	implicit power law (conv) central diff (cond)
Yang & Garimella (2013) [17] Yang & Garimella (2010) [18] Flückiger et al. (2013) [19]	HITEC quartzite	50–100	non dim	non dim	2.88–32.1 / 2–5	single blow	2D-CS impulse eq. FV FLUENT	static fluid	no	1 1e-3	yes, iterative	2nd order implicit 2nd order upw. (conv) central diff (cond)
Hoffmann et al. (2016) [20]	rapseed oil Caloria HT Solarsalt rocks (var)	40 / 0.41 19.1 / 0.22 4.5 / 0.22	160 / 210 298 / 295.9 179.2 / 295.5	8.3 kWh 2.3 MWh 170 MWh	1.8 / 0.4 6.1 / 3 12 / 18.2	single blow	1D-SP plug flow FD MATLAB	static	yes with fluid	4000n ?	yes (4 min update)	implicit 2nd order (both)
Hoffmann et al. (2016) [20]	rapseed oil, Caloria HT Solarsalt, rocks (var)	40 / 0.41 19.1 / 0.22 4.5 / 0.22	160 / 210 298 / 295.9 179.2 / 295.5	8.3 kWh 2.3 MWh 170 MWh	1.8 / 0.4 6.1 / 3 12 / 18.2	single blow	1D-CS plug flow FD MATLAB	static solid & fluid	yes PDL	4000n ?	yes (4 min update)	implicit 2nd order (both)
Valmiki et al. (2012) [21]	Xceltherm 600 river pebbles, pea pebbles	20 / 0.326 5 / 0.326	~20 / 140	11 kW 0.75–2 l / min	0.767 / 0.241	cyclic	1D-SH plug flow -	no	no	? ?	?	? ?
Van Lew et al. (2009) [22] Li et al. (2011) [23] Reddy et al. (2017) [24]	non-dim	? / 0.25	non dim	non dim	non dim	cyclic	1D-SH plug flow -	no	no	20, 100, 1000n ?	no	2nd order trapezoidal rule
Galione et al. (2015) [25]	molten salt rocks PCM	15 / 0.22 15 / 0.34	290 / 390	~ 2–4 MWh 5.85 kg/s	? / 5.2	cyclic (multiple)	1D-DC plug flow FV	static & dynamic fluid	yes	92n x 52n var. time step	yes	1st order explicit ?
Votyakov et al. (2014) [26] *Bonanos* et al. *(2016)* [27]	non dim	2.5–300	non dim	$Pe = 5000$	6 / 0.22	single blow	2D-CS perturbation plug flow -	static fluid	no	analytical	no	analytical
Bayon et al. (2013) [28]	molten salt, oil sand, rocks	? / 0.22 ? / 1	300 / 550	0.1–1 MW -	0–16 /?	single blow	1D-SP plug flow MATLAB	static fluid	yes	500n	no	Matlab ode45 power law scheme
Yin et al. (2017) [29]	molten salt zirkonium balls, SiC	12 / 0.65	290 / 370	- ~ 0.68 kg/s	0.45 / 0.12	single blow	2D-CS impulse eq FLUENT	static fluid	no	? ?	yes	? ?
Flückiger et al. (2014) [30]	quartzite	10 / 0.22	300 / 600	2500 MW -	11.0 / 36.27	annual	1D-CS plug flow FV	static fluid	no	2.2 cm 3 s	yes (Picard iteration)	1st order implicit 2nd order & flux limiter
Yang et al. (2012) [31]	HITEC fictive	30 / 0.4 6 / 0.4 20 / 0.2	260 / 355	- 0.87 kg/s	0.55 / 0.236	single blow	1D-CS plug flow FD	static solid & fluid	yes PDL	800,1600,2000n ?	no	implicit central diff. (cond) upw. (conv)

(*continued on next page*)

Table 5 (*continued*)

[1]Publication	Material fluid solid	Particles d[mm] / eps[–]	Temp. [°C] low / high	Size mass flow	Storage volume height [m] / diameter [m]	Operation	Model flow [2]discretization	Eff cond	Heat loss	[3]Grid size time step	Variable properties	[4]Numerical solution
Xu et al. (2012) [32]	solarsalt quartzite rock	19.05 / 0.22	290 / 390	50 MWh -	14 / 8.6	cyclic	2D-CS impulse eq. FV	static solid & fluid	yes PDL	82n x 65n 5 s	yes	implicit 2nd order (conv) central diff. (cond)
Xu et al. (2013) [33]	solarsalt various fillers	10–250 / 0.22	290 / 390	50 MWh 70 kg/s	14 / 8.6	cyclic	2D-DC impulse eq. FV	static & dynamic fluid	yes PDL	82n x 65n 5 s	yes	implicit 2nd order (conv) central diff. (cond)
Niedermeier et al. (2018) [34]	molten salts quartzite	5–50 / 0.1–0.9	700 / 500	40 MWh -	~11 / var	cyclic stand-by	1D-CS plug flow FV	static solid & fluid	no	500 4.8 s	no	2nd order CN 1st order upw. (conv) central diff. (cond)
Niedermeier et al. (2018) [34]	pure sodium quartzite	5–50 / 0.1–0.9	700 / 500	40 MWh -	~11 / var	cyclic stand-by	1D-DC plug flow FV	static solid & fluid	no	1000 × 70 2.9 s	no	2nd order 1st order upw. (conv) central diff. (cond)
Kocak and Paksoy (2019) [35]	Therminol 66 demolition waste	10 / 0.45	24 / 90	- 1000 kg/h	0.9 / 0.3	single blow	1D-SH/CS plug flow FD	dynamic solid & fluid	no	90 ?	no	? ?

[1] other publications in italic [2] FD = finite differences, FV = finite volume, [3] n = nodes, [4] cond. = conduction, conv. = convection, upw. = upwind, CN=Crank-Nicholson.

Table 6
Summary of boundary conditions.

	Common boundary conditions				
Solarfield outlet temperature	550				°C
Solarfield peak thermal power †	793				MW
Solarfield max. mass flow rate †	1500				kg/s
Power block outlet temperature	312 (310)				°C
Power block thermal power	235				MW
Power block net electric power †	97.5				MW
Power block mass flow rate	630				kg/s
Min. thermal energy threshold in storage for discharge or power block active †	235				MWh
Ambient and ground temperature ‡	20				°C
Total heat transfer coefficient ‡	0.2				W/m^{2}K
	Storage specifications				
Size	6 h/80 K		12 h/40 K		
Storage time	6		12		h
Permitted change in exit temperature	80		40		K
Packings	2–2/0.40	2–50/0.22	2–2/0.40	2–50/0.22	
Particle diameters d_{p1}/d_{p2} (mixture)	2	2 & 50	2	2 & 50	mm
Share of large filler	–	70	–	70	%
Mean particle diameter	2	35.6	2	35.6	mm
Total void fraction	40	22	40	22	%
	Sizing of the storage volumes				
Length	10				m
Cross sectional area	720	800	1480	1920	m^2
Storage diameter	30.3	31.9	43.4	49.4	m
Total inner surface of tank	2392	2602	4323	5392	m^2
Mass flux density	0.875	0.788	0.426	0.328	kg/m^{2}s

† relevant for annual simulations.
‡ relevant for heat losses.
* for simplicity, single blow and cyclic simulations are initialized and run with 310°C as lower temperature.

grid size of 0.05 cm (20,000 nodes) is used for the simulations. For better distinction of the curves, a magnification of the region with largest differences is given.

In the case of the larger 2–50/0.22 particles (Fig. 8, left), there is almost no further improvement in accuracy between the time step length of 0.02 and 0.05 s for the SH model. Hence, the simulation with 0.02 s time step length can be considered as "exact" solution and taken as reference. Comparing the curves to the reference, a time step length of 2.0 s seems a reasonable compromise between precision and computational time. In this case, the mean temperature difference to the reference $\Delta\overline{T_f}$ is around 0.1 Kelvin and the maximum difference $\Delta T_{f,\,max}$ around 0.2 Kelvin, as given by Table 4.

A demanding situation is the simulation of the small particles 2–2/0.40 (Fig. 8, right) due to its sharp thermal gradient. This generally leads to large differences and even numerical instabilities at time steps of 0.1 s and below. To avoid those instabilities, grid size would have to be reduced further, increasing computing time which is already high (up to ~5000 s for 3 h of real time). Since the sharp gradient will vanish during cyclic operation and annual simulations, a time step length of 0.2 s for the cyclic operation and 0.5 s for annual simulations can be accepted. Due to the steep gradient, mean and maximum temperature difference are still high, $\Delta\overline{T_f}$ is around 30 Kelvin and the maximum difference $\Delta T_{f,\,max}$ around 40 Kelvin, see Table 4.

Additionally, simulations are run with the bidisperse model, see Table 4. Albeit small particles contribute to a steeper temperature profile, the larger particles have a damping effect on the thermal gradient,

Table 7
Summary of the single blow and hold simulations; mean and maximum temperature differences for a variation of the models with Schumann (SH) as reference; bidisperse and monodisperse packing investigated with two different storage configurations.

Storage	6 h / 80 K				12 h / 40 K			
PEC	$\Delta\overline{T_f}$/K		$\Delta T_{f,max}$ / K		$\Delta\overline{T_f}$/K		$\Delta T_{f,max}$ / K	
Time	3 h	3 h + 24 h	3 h	3 h + 24 h	6 h	6 h + 24 h	6 h	6 h + 24 h
Bidisperse packing (2–50/0.22)								
SH (ref)	–	–	–	–	–	–	–	–
SH-VP	0.929	0.906	6.438	6.377	0.713	0.697	6.939	6.870
CS	0.119	1.035	0.594	4.943	0.338	1.585	2.415	10.199
CS-WL	0.163	1.675	0.646	18.027	0.420	2.207	2.400	18.001
BD	1.294	1.288	6.895	6.281	0.882	0.880	6.651	6.090
Monodisperse packing (2–2/0.40)								
SH (ref)	–	–	–	–	–	–	–	–
SH-VP	0.177	0.177	14.410	14.400	0.184	0.184	19.816	19.810
CS	0.766	3.582	29.500	71.278	1.474	4.058	54.940	82.817
CS-WL	0.808	4.342	29.459	71.308	1.529	4.746	54.879	82.552
SP	0.439	3.460	18.922	70.322	1.332	3.993	52.000	82.432

leading to even lower temperature differences as seen in the single-phase model. Thus, for the BD model the same time step of 0.2 s as for the SH model can be used.

4.1.4. Variation of grid size

In the next study, grid size is varied. Fig. 9 shows the calculated temperature curves for the Schumann (SH) and single-phase (SP) models.

In terms of the SH model, a grid spacing of 2 cm (500 nodes) seems a reasonable compromise. In this case, $\Delta\overline{T_f}$ is around 0.7 Kelvin and $\Delta T_{f,max}$ around 1.1 Kelvin, as highlighted in Table 4.

For the SP model, the situation is again challenging due to the harsh thermal gradients. In this case, the temperature curve almost equals a step function, since effective conductivity has only little smoothing effect. If a step function should be expressed, tiny time steps would be necessary, which also forces a reduction in grid spacing. Here, even at the lowest grid size of only 0.05 cm, a small instability occurs. With larger grid spacing, those instabilities reach inacceptable size. Hence, for the following simulations, the smallest grid size of 0.05 cm is maintained. However, due to the increased computing time, for the annual simulation of small particles (2–2/0.40) an exception will be made. In this case, a grid size of 0.2 cm will be used, reducing the expected computing time to one week instead of four. This can be justified since a step change only occurs within the beginning of the simulations. Again, Table 4 shows rapidly increasing $\Delta\overline{T_f}$ and $\Delta T_{f,max}$ values for the SP model.

The situation for the bidisperse model is again similar to the variation of time step and only differs little from the SH model. Thus, a grid spacing of 2 cm is used as well. Data is also given by Table 4.

4.1.5. Suitability of the models for different packing size distributions

In this section we evaluate the general impact of particle sizes on the model outcome. The focus lies on the effect of the utilization of one, two or three PDEs, thus only single-phase (SP) and bidisperse (BD) model are compared to the Schumann model (SH). Since effective conductivity is used within the single-phase model, the continuous-solid-phase (CS) model is also considered for comparison. For the evaluation the cyclic operation is used. The absolute difference of said models to the reference (SH) is plotted for both the smaller 6 h/80 K and the larger 12 h/40 K storage configuration in Fig. 10; the actual values are summarized in Table 8.

Effective conductivity has a visible impact in two cases: First, there is a trend towards smaller particles, which can be seen in Fig. 10. Smaller particles have a better heat transfer causing a narrow thermocline zone and thus a higher temperature gradient. This temperature gradient is driving conductive heat transfer and widening the thermocline. For this reason, differences to the SH model are higher with small particles.

Secondly, the effect is more distinct within the 12 h/40 K configuration, which is also clearly visible in Fig. 10. The convective contribution is smaller due to the lower mass flux density which is only about half as high. Furthermore, the permitted drop in exit temperature is lower, which allows the thermocline to develop further.

Single-phase: At the small particle sizes the single-phase model shows a good agreement with the CS model, since both utilize effective conductivity. However, already at slightly larger particle sizes of the 2–18/0.34 packing, the deviation rapidly increases (deviation to the CS model is even higher, since values for the SP model get negative). Thus, the single-phase model should not be considered with larger particles than a few millimeters. Therefore, it is well justified to omit the single-phase model in the investigations of all bidisperse packings.

Two solid phases: The bidisperse model expectedly equals the SH model for the 2–2/0.40 packing. Therefore, it is justified to omit the bidisperse model for the investigation of all monodisperse packings. There is a linear trend of the deviations towards larger particles which is for the 2–50/0.22 packing about 1.6% within the 6 h/80 K configuration and 3.2% within the 12 h/40 K configuration. Similar to the effect of effective conductivity, the deviations are higher, when there is more room for the development of the thermocline as in the 12 h/40 K configuration. Thus, if the larger particles within a packing exceed about 10 to 20 mm, the bidisperse model adds more precision to the model outcome than the effective conductivity which impact is further declining with larger particles. The actual differences are summarized in Table 8.

4.2. Single blow and hold

The following section shows computed temperature curves of the single blow and hold operation. This means that the storage is half charged, i.e. operated for the duration of 50% of one period, beginning from uniform temperature (single blow). After that operation is followed by an idle time, i.e. no mass flow, for 24 h (hold phase). The temperature curves are plotted in several figures and the mean and maximum deviations are summarized in Table 7.

Generally, the Schuman model (SH) is taken as the reference case. As stated in section 3.2, the bidisperse model (BD) is considered only for the bidisperse packing and the single-phase (SP) model only for the monodisperse packing.

Table 8
Summary of cyclic simulation; difference in total cycling duration for a variation of the models with Schumann (SH) as reference; range of packings investigated with two different storage configurations.

Storage	6 h / 80 K (760 m²cross sectional area)								12 h / 40 K (1700 m²cross sectional area)							
Packing	2–2/0.40		2–18/0.34		2–34/0.28		2–50/0.22		2–2/0.40		2–18/0.34		2–34/0.28		2–50/0.22	
PEC	Δt_{fcd} / s	Δt_{fcd} / %	Δt_{fcd} / s	Δt_{fcd} / %	Δt_{fcd} / s	Δt_{fcd} / %	Δt_{fcd} / s	Δt_{fcd} / %	Δt_{fcd} / s	Δt_{fcd} / %	Δt_{fcd} / s	Δt_{fcd} / %	Δt_{fcd} / s	Δt_{fcd} / %	Δt_{fcd} / s	Δt_{fcd} / %
SH (ref)	618,658	–	597,880	–	577,238	–	556,516	–	1,360,788	–	1,250,042	–	1,149,080	–	1,055,458	–
CS (diff)	3910	0.63	1462	0.24	948	0.16	734	0.13	57,492	4.22	23,964	1.92	14,802	1.29	10,784	1.02
SP (diff)	2336	0.38	−21,738	−3.64	−45,632	−7.91	−69,516	−12.5	53,038	3.90	−62,268	−4.98	−167,386	−14.6	−264,654	−25.1
BD (diff)	0	0.00	2824	0.47	5890	1.02	8972	1.61	0	0.00	13,332	1.07	24,796	2.16	34,288	3.25

4.2.1. *Bidisperse packing (2-50/.22)*

Fig. 11 shows the fluid temperatures of the single blow and hold simulations for the bidisperse packing with 2–50 mm particles and 22% void fraction (2–50/0.22). The diagrams on the left side are plotted after 50% of the duration of one period (single blow), which is 3 h and 6 h for the for the 6 h/80 K and 12 h/40 K configurations, respectively. The curves on the right were plotted after the additional hold phase of 24 h without flow.

Generally, it can be observed that during hold phase all temperature curves are shifting slightly backwards even those for models without effective conductivity. This effect is caused by the ongoing heat transfer from the fluid to the solid at the beginning of the hold phase when the flow is reduced to zero.

Effective conductivity: The impact of effective conductivity becomes visible when comparing the continuous-solid-phase model without wall loss (CS) to the Schumann model (SH). After single blow operation, the differences remain small for both configurations. As given by Table 7, the mean temperature difference $\Delta\overline{T_f}$ is approx. 0.3 K for the 6 h/80 K-storage configuration and 1.3 K for the 12 h/40 K-storage configuration. The reason for the greater difference in the latter storage configuration is due to the smaller convective term, thus the influence of conduction is higher. However, effective conductivity becomes significant during the hold phase, as the differences grow further to around 3.1 K and 6.7 K, respectively.

Wall loss: The effects of wall losses appear negligible during the single blow phase, which can be seen by comparing the continuous-solid-phase models with (CS-WL) and without wall loss (CS). Mean temperature differences $\Delta\overline{T_f}$ are below 0.2 Kelvin in all cases. During the hold phase, however, the comparatively large surface at the bottom and top of the storage volume causes a significant temperature drop, which can be clearly seen in Fig. 11. The maximum temperature differences occurring now reach up to 18 K for both configurations.

Variable fluid properties: The utilization of variable fluid properties (SH vs. SH-VP) is causing a mean temperature difference $\Delta\overline{T_f}$ of approximately 0.9 K and 0.7 K for the 6 h/80 K- and 12 h/40 K-configurations, respectively, which is also maintained during the hold phase. Thus, considering variable fluid properties has a significantly larger effect than considering effective conductivity. Another interesting salience is that the shape of the temperature profile becomes asymmetric when variable fluid properties are enabled. That is because for the SH-VP model the actual heat capacity of the rocks in the colder region is lower than the mean value and vice versa in the hot regions.

Two solid phases: When considering two solid phases, as in the bidisperse model (BD), the largest differences to the reference case (SH) appear. The mean temperature difference $\Delta\overline{T_f}$ is about 1.9 K and 1.4 K for the 6 h/80 K- and 12 h/40 K-configurations, respectively.

4.2.2. *Monodisperse packing (2-2/.40)*

The simulations are repeated with mono-sized particles of 2-mm. Fig. 12 shows calculated fluid temperature curves for the monodisperse packing with 2-mm particles and 40% void fraction (2–2/0.22). Again, the diagrams on the left side are plotted after single blow and on the right after the additional hold phase of 24 h without flow.

Effective conductivity: The continuous-solid-phase model without wall loss (CS) compared to the Schumann model (SH) shows a mean temperature difference $\Delta\overline{T_f}$ of 0.8 K and 1.5 K for the 6 h/80 K- and 12 h/40 K-configurations, respectively. Whilst effective conductivity had the lowest impact at the bidisperse packing, it now causes the largest differences. The reason for this is that conductivity is driven by temperature gradients inside the bed, which are significantly higher for the small particles. After the stand-by period the differences grow significantly further to around 3.6 K and 4.1 K, respectively. Since the curves have a steep slope, the maximum local temperature differences are comparatively high, reaching >71 K and 82 K, respectively.

Table 9
Summary of the cyclic operation; difference of the last periods and total cycling duration for a variation of the models with Schumann (SH) as reference; bidisperse and monodisperse packing investigated with two different storage configurations.

Storage	6 h / 80 K						12 h / 40 K					
PEC	$\Delta t_{per}'$ / s	$\Delta t_{per}'$ / %	$\Delta t_{per}''$ / s	$\Delta t_{per}''$ / %	Δt_{tcd} / s	Δt_{tcd} / %	$\Delta t_{per}'$ / s	$\Delta t_{per}'$ / %	$\Delta t_{per}''$ / s	$\Delta t_{per}''$ / %	Δt_{tcd} / s	Δt_{tcd} / %
Bidisperse packing (2–50/0.22)												
SH (ref)	21,588	–	21,586	–	585,878	–	42,996	–	42,990	–	1,201,550	–
SH-VP (diff)	−132	−0.61	86	0.40	−548	−0.09	−296	−0.69	−110	−0.26	−2296	−0.19
CS (diff)	30	0.14	30	0.14	786	0.13	562	1.31	562	1.31	14,194	1.18
CS-WL (diff)	28	0.13	36	0.17	838	0.14	596	1.39	628	1.46	15,242	1.27
BD (diff)	350	1.62	350	1.62	9234	1.58	1488	3.46	1488	3.46	37,626	3.13
Monodisperse packing (2–2/0.40)												
SH (ref)	21,797	–	21,796.8	–	588,761	–	44,087.8	–	44,087	–	1,193,849	–
SH-VP (diff)	−1	0.00	24.8	0.11	371	0.06	41.8	0.09	57.6	0.13	2036.6	0.17
CS (diff)	173.2	0.79	173.2	0.79	4513.2	0.77	2093.8	4.75	2094.6	4.75	51,005.8	4.27
CS-WL (diff)	173	0.79	174.2	0.80	4522.4	0.77	2100.4	4.76	2107	4.78	51,194.2	4.29
SP (diff)	99	0.45	99	0.45	2581.8	0.44	1894	4.30	1894.8	4.30	46,135.2	3.86

Table 10
Summary of the annual simulations; difference in produced electricity and extracted exergy from storage during discharging for a variation of the models with Schumann (SH) as reference; bidisperse and monodisperse packing investigated with two different storage configurations.

Storage	6 h / 80 K				12 h / 40 K			
PEC	ΔE_{el}/ GWh	ΔE_{el}/ %	$\Delta E_{stor}''$/ GWh	$\Delta E_{stor}''$/ %	ΔE_{el}/ GWh	ΔE_{el}/ %	$\Delta E_{stor}''$/ GWh	$\Delta E_{stor}''$/ %
Bidisperse packing (2–50/0.22)								
SH (ref)	398.8	–	344.3	–	494.7	–	540.3	–
SH-VP (diff)	0.3	0.08	0.4	0.12	−0.4	−0.08	−1.1	−0.20
CS (diff)	−0.5	−0.13	−1.1	−0.32	−1.9	−0.38	−4.0	−0.74
CS-WL (diff)	−1.2	−0.30	−2.2	−0.64	−3.9	−0.79	−7.4	−1.37
BD (diff)	−3.4	−0.85	−6.9	−2.00	−4.6	−0.93	−9.7	−1.80
Monodisperse packing (2–2/0.40)								
SH (ref)	412.4	–	369.7	–	503.8	–	555.2	–
SH-VP (diff)	0	0.00	−0.1	−0.03	−0.2	−0.04	−0.4	−0.07
CS (diff)	−2.2	−0.53	−4.7	−1.27	−6.9	−1.37	−14.2	−2.56
CS-WL (diff)	−2.7	−0.65	−5.6	−1.51	−8.3	−1.65	−17.0	−3.06
SP (diff)	−1.6	−0.39	−3.4	−0.92	−6.4	−1.27	−13.1	−2.36

Table 11
Qualitative impact of different models and assumptions depending on use case, storage size and packing configuration.

	Packing	Single blow		Hold † (stand-by)		Cyclic operation		Annual simulation	
Performance evaluation criterium (PEC)		Mean temp. Difference $\Delta\overline{T_f}$		Mean temp. Difference $\Delta\overline{T_f}$		Difference in total duration Δt_{tcd}		Recovered exergy $\Delta E_{stor}''$	
Storage size		6 h / 80 K	12 h / 40 K	6 h / 80 K	12 h / 40 K	6 h / 80 K	12 h / 40 K	6 h / 80 K	12 h / 40 K
Variable fluid properties	2–50/0.22	Med	Med	Low	Low	Low	Low	Low	Low
(SH-VP)	2–2/0.40	Low	Low	Low	Low	Low	Low	Low	Low
Effective conductivity	2–50/0.22	Low	Low	Low	Med	Low	Low	Low	Low
(CS)	2–2/0.40	Med	High	High	High	Low	High	Med	High
Wall losses*	2–50/0.22	Low	Low	Low	Low	Low	Low	Low	Low
(CS-WL)	2–2/0.40	Low	Low	Low	Low	Low	Low	Low	Low
Single phase*	2–50/0.22	–	–	–	–	–	–	–	–
(SP)	2–2/0.40	Low	Low	Low	Low	Low	Low	Low	Low
Bidisperse	2–50/0.22	High	Med	Low	Low	Med	High	Med	Med
(BD)	2–2/0.40	–	–	–	–	–	–	–	–

*rating relative to the CS-model (to subtract influence of effective conductivity, see section 3.4).
† differences relative to the end of single blow operation (includes only impact of hold phase, see section 3.4).

Wall loss: The effects of wall losses again are small during the single blow phase (CS-WL vs. CS). Mean temperature differences $\Delta\overline{T_f}$ are below 0.1 Kelvin in all cases. The mean temperature differences are also not as high as before during the hold phase, which is caused by the generally larger differences due to the steep temperature profiles. The impact of wall losses at the end nodes, however, is still significantly large, as can be seen in Fig. 12 in the right diagrams.

Variable fluid properties: The utilization of variable fluid properties (SH vs. SH-VP) is causing a mean temperature difference $\Delta\overline{T_f}$ of approximately 0.2 K for both configurations, which is also maintained

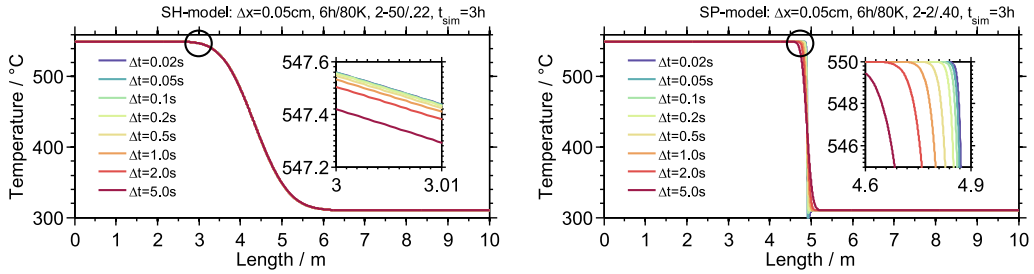

Fig. 8. Grid study with 0.05 cm spatial discretization, variation of time step length. Left: Schumann model (SH), right: single-phase model (SP).

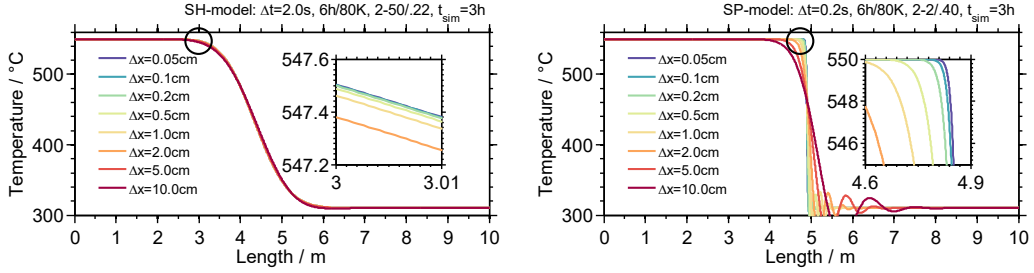

Fig. 9. Grid study with variation of spatial discretization. Left: Schumann model (SH), right: single-phase model (SP).

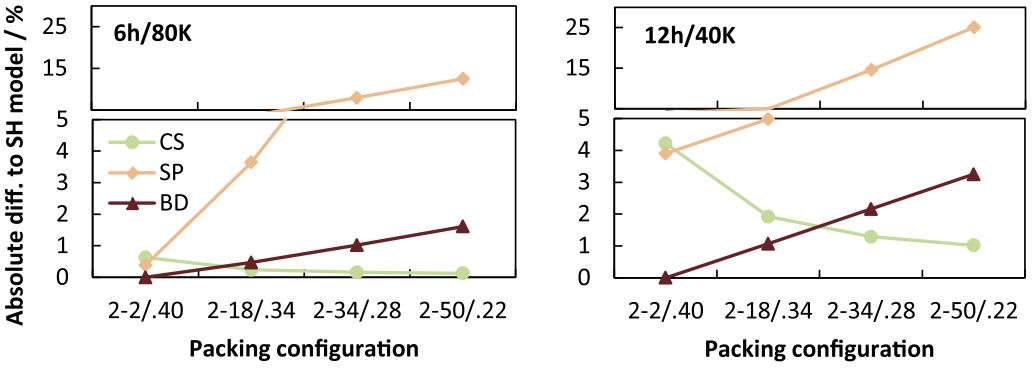

Fig. 10. Absolute difference in total cycling duration of the CS, SP and BD models to the reference model (SH) for variation of the particle sizes in percent. Left: 6 h/40 K-configuration, right: 12 h/40 K-configuration.

during the hold phase. Compared to the simulations with the bidisperse packing, this is significantly smaller and has the lowest impact among the monodisperse packing.

Single-phase: The single-phase model (SP) temperature curves are close to those of the continuous-solid-phase model (CS). As observed in the CS model beforehand, the effective conductivity has a dominant effect due to the large temperature gradients. The mean temperature difference compared to the Schumann model (SH) $\Delta\overline{T_f}$ is about 0.4 K and 1.3 K for the 6 h/80 K- and 12 h/40 K-configurations. Compared to the CS model, $\Delta\overline{T_f}$ are as low as 0.3 K and 0.1 K, respectively.

4.3. Cyclic operation

In this section the outcome of the models after cyclic operation for 14 cycles is compared. Since the harsh temperature differences occurring in the single blow operation have now time to average out, their effects should vanish in this investigation. Temperature plots have been omitted since they would significantly differ in their spatial position after several cycles. For performance evaluation, time differences of the last periods $\Delta t_{per}'$ and $\Delta t_{per}''$ as well as total duration Δt_{tcd} compared to the reference case are used (see section 3.2.2). The results are summarized in Table 9.

4.3.1. Bidisperse packing (2-50/.22)

Effective conductivity: The impact of effective conductivity is now strongly depending on its relation to the influence of convection. It has only little effect within the 6 h/80 K-configuration, where mass flux density is high: the last periods $\Delta t_{per}'$ and $\Delta t_{per}''$ last only 30 s longer, but for the 12 h/40 K-configuration the last periods are 562 s longer. This has also been visible in the single blow operation before.

Wall loss: The impact of wall losses appears almost negligible, which is consistent to the findings of the single blow operation. Due to the heat losses, the exit temperature is slightly reduced and the threshold for the switching condition should be reached later. Thus, the last charging periods $\Delta t_{per}'$ should last a few seconds longer than the discharge periods $\Delta t_{per}''$, which is the case as shown in Table 9.

Variable fluid properties: Since variable fluid properties cause local differences in heat capacity and density as observed in the single blow operation, the effect should be larger for the 12 h/40 K-configuration having the higher thermal capacity, which is the case. The effect, however averages out due to the cycling and becomes less dominant as in the single blow operation. Furthermore, variable fluid properties have an impact on the progression of the outlet temperature and thus thermal power. This leads to a slightly shorter charging period $\Delta t_{per}'$ than the discharging period $\Delta t_{per}''$.

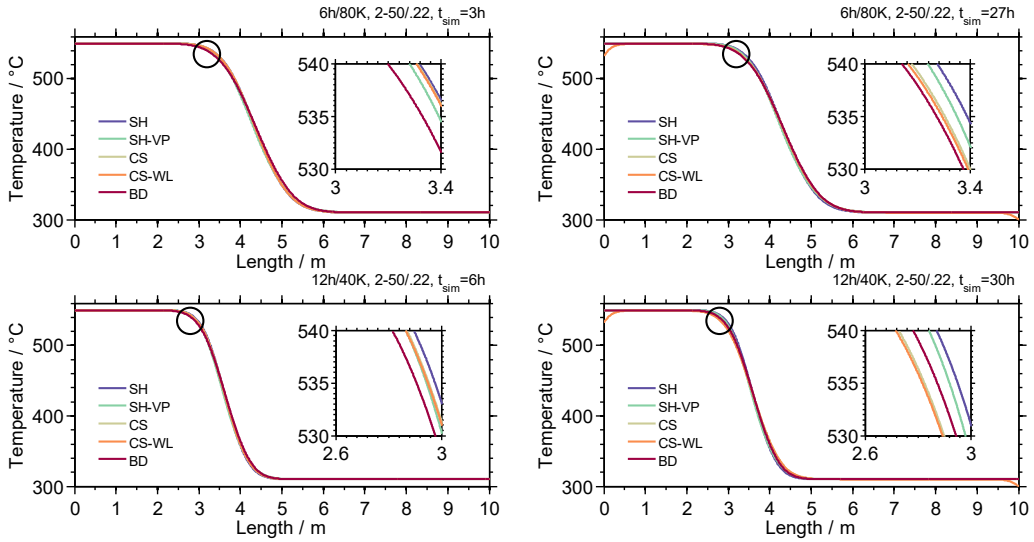

Fig. 11. Comparison of the different models after single blow operation (left) and after additional 24 h of hold phase (right). Particle size 35.6 mm (SH & CS models) and 2.0/50.0 mm (BD model). Top: 6 h/80 K-configuration, bottom: 12 h/40 K-configuration.

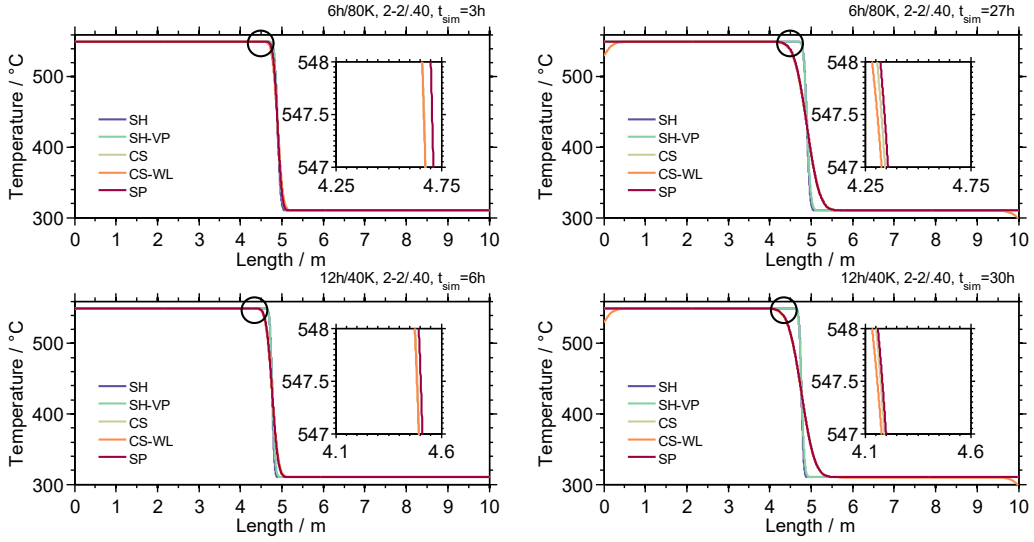

Fig. 12. Comparison of the different models after single blow operation and after additional 24 h of hold phase. Particle size 2.0 mm for all models, Top: 6 h/80 K-configuration, bottom: 12 h/40 K-configuration.

Two solid phases: The bidisperse model again has the highest impact on the modelling outcome. The last periods are increased by about six minutes which sums up to a total extension of total cycling duration Δt_{tcd} of 2.5 h for the 6 h/80 K-configuration. The impact on the 12 h/40 K-configuration is even higher, with an increase of period length $\Delta t_{per}'$ and $\Delta t_{per}''$ of 25 min and total duration Δt_{tcd} by 10.5 h.

4.3.2. *Monodisperse packing (2-2/.40)*

Effective conductivity: The impact of effective conductivity is highest for the monodisperse packings, which has already been visible at the single blow simulations. The period lengths increase only by three minutes for the 6 h/80 K-configuration but by 35 min for the 12 h/40 K-configuration, where convection is lower.

Wall loss: The same observations as from the bidisperse packing are visible as well. Again, the impact of wall losses is negligible and ranges only within a few seconds difference in period length.

Variable fluid properties: The observation of different charging and discharging time can be repeated for the monodisperse packing. Total cycling duration is now increased in contrast to the bidisperse packing. This indicates that solid/fluid ratio has an impact as well.

Single-phase: Since effective conductivity is considered in the single-phase model, the profile is mainly influenced by conduction. Comparing the model outcome to the CS model, conduction causes >50% of the differences in the 6 h/80 K-configuration and almost 90% in the 12 h/40 K-configuration.

4.4. *Annual simulation*

In the final section, the model outcome for a complete year is compared to the Schumann model. Since heat supply is different every day, it is not ensured that the storage can be fully charged. Moreover, every day is containing stand-by periods. Thus, this use case represents a mixture of the use cases before. The discussion is based on a graphical representation of the full load hours of each day of the year for the SH model and the respective differences of the other models (see Fig. 13 and Fig. 14). The overall outcome is given in absolute and relative values for

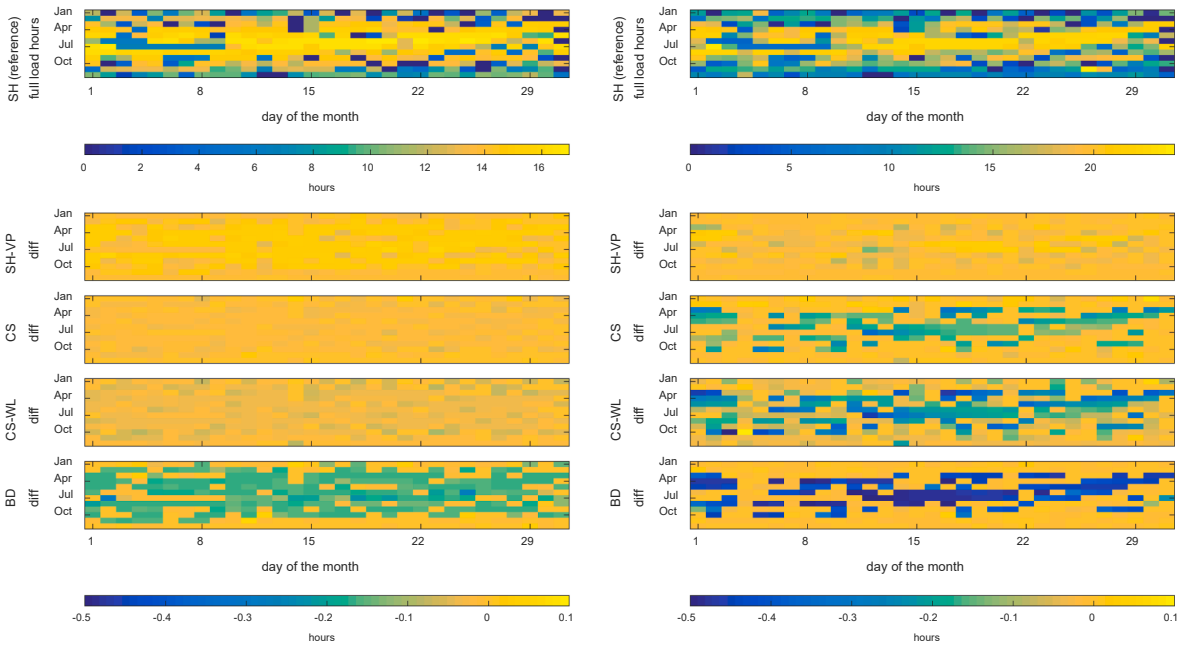

Fig. 13. Full load hours per day of Schumann model (reference) and absolute difference of other models for the bidisperse packing (2–50/0.22). Left: 6 h / 80 K storage configuration, right: 12 h / 40 K storage configuration.

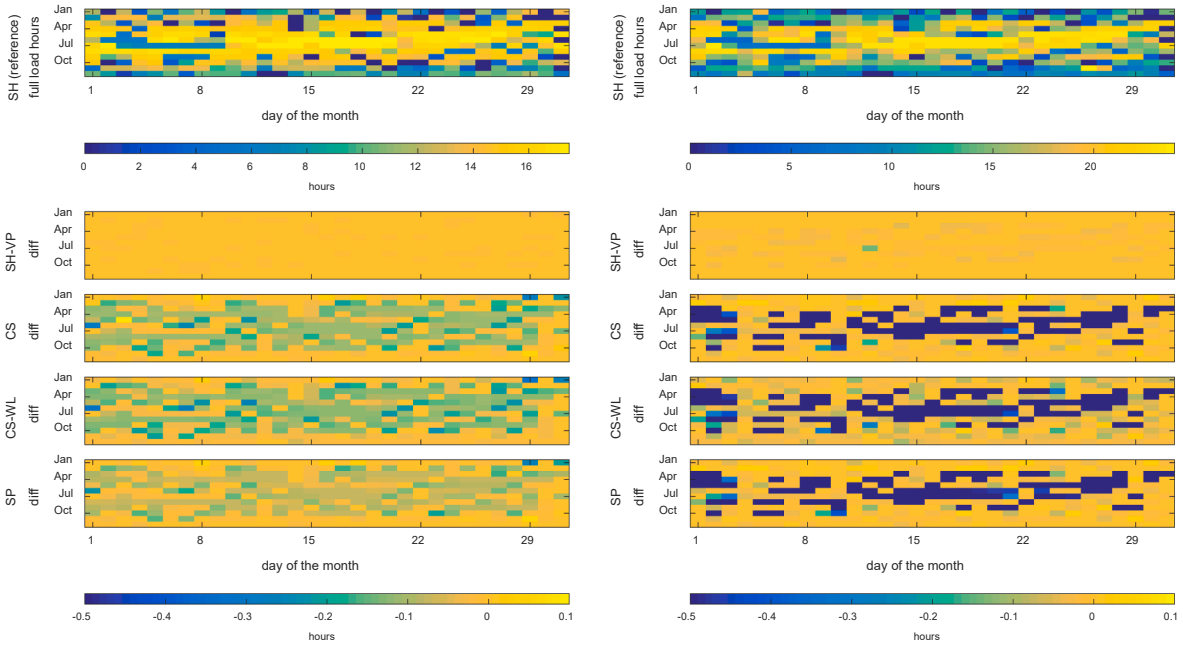

Fig. 14. Full load hours of Schumann model (reference) and absolute difference of other models for the monodisperse packing (2–2/0.40). Left: 6 h / 80 K storage configuration, right: 12 h / 40 K storage configuration.

produced electricity ΔE_{el} and recovered exergy $\Delta E_{stor}''$ as summarized in Table 10.

4.4.1. *Bidisperse packing (2-50/.22)*

The full load hours of the bidisperse packing are illustrated in Fig. 13.

Effective conductivity has only a minor impact on the annual model outcome, particularly for the smaller 6 h/80 K-configuration. For the larger 12 h / 40 K storage configuration, there are several days in the summer months, where operation time per day is rather long (> 20 h). During these days, there is enough time given where effective conductivity of the bed widens the thermocline zone, thus reducing the operation time by up to 0.2 h. Since this effect is occurring only at some specific days during the summer time, the produced electricity ΔE_{el} reduces by 1.9 GWh and exergy from the storage $\Delta E_{stor}''$ by 4 GWh or 0.38% and 0.74%, respectively.

Wall loss: By adding wall loss to the CS model, the reduction in full load hours is approximately doubled for both storage configurations. This can also be seen in the produced electricity ΔE_{el} or recovered exergy

from the storage $\Delta E_{stor}''$. For the larger storage volume (12 h / 40 K), 3.9 GWh less electricity (−0.79%) and 7.4 GWh (−1.37%) less exergy is regained from the storage.

On October the 3rd, there was significantly less production of electricity of −2.7 full load hours which was then followed by a significantly higher production the next day. The reason was that due to the additional losses, the minimum threshold for the power block activation was not met.

Variable fluid properties appear to have the least impact on the annual model outcome, as harsh temperature gradients do not occur anymore. However, as already observed at the cyclic operation, variable fluid properties cause a slight increase in full load hours for the 6 h / 80 K storage configuration, the total effect, however, is rather small: ΔE_{el} increases by 0.3 GWh (+ 0.08%), $\Delta E_{stor}''$ by 0.4 GWh (+ 0.12%). For the larger 12 h / 40 K storage configuration, the effect is opposed, ΔE_{el} decreases by 0.4 GWh (− 0.08%) and $\Delta E_{stor}''$ by 1.1 GWh (− 0.2%).

Two solid phases: The introduction of the second solid phase has the highest impact. Full load hours of the 6 h / 80 K storage configuration reduce up to 0.2 h per day, which reduces ΔE_{el} by 3.4 GWh (− 0.85%), and $\Delta E_{stor}''$ by 6.9 GWh (− 2.0%). For the larger storage (12 h / 40 K), there are fewer but generally more distinct days with a significant reduction in full load hours. The differences can reach up to 0.5 h in that case. Since the bidisperse model is more accurate in modelling the lower heat transfer of the larger particles, the effect is occurring on those days where the thermocline is given most time to develop. This usually happens in the summer days. In total ΔE_{el} is reduced by 4.6 GWh (−0.93%) and $\Delta E_{stor}''$ by 9.7 GWh (−1.8%).

4.4.2. Monodisperse packing (2-2/.40)

Finally, we discuss the outcome of the monodisperse packing.

Effective conductivity: From comparing full load hours for the monodisperse packing (Fig. 14) to the bidisperse packing (Fig. 13), it can be seen that effective conductivity is now having a more distinct effect. The reason for this lies in the higher temperature gradient through the steeper progression of the thermocline profile which is enhancing conductive heat transfer. Full load hours are up to 0.2 h less for the smaller 6 h / 80 K storage configuration which is for ΔE_{el} 2.2 GWh less (−0.53%) or 4.7 GWh (−1.27%) for $\Delta E_{stor}''$.

For the larger 12 h / 40 K configuration, differences are much higher, reaching a reduction in full load hours of up to 1.5 h on some days. ΔE_{el} is reduced by 8.3 GWh (−1.65%) and $\Delta E_{stor}''$ by 14.2 GWh (−2.56%).

Wall loss: Adding wall losses has apparently only little impact for the monodisperse packing. Fig. 14 shows no visible difference. For both storage configurations the reduction of produced electricity and exergy from the storage differs only slightly as shown in Table 10.

Variable fluid properties have the lowest impact for the monodisperse packing. Full load hours are almost not affected as well as produced electricity ΔE_{el} or recovered exergy from the storage $\Delta E_{stor}''$, where all differences are below 0.1%.

Single-phase: The single-phase model shows a quite similar result as the CS model. Full load hours are also up to 0.2 h less for the smaller 6 h / 80 K storage configuration which is for ΔE_{el} 1.6 GWh less (−0.39%) or 3.4 GWh (−0.92%) for $\Delta E_{stor}''$.

For the larger 12 h / 40 K configuration, differences are much higher as well, where full load hours are up to 1.5 h less on some days. ΔE_{el} is reduced by 6.4 GWh (−1.27%) and $\Delta E_{stor}''$ by 13.1 GWh (−2.36%).

Since the single-phase (SP) model also considers effective conductivity, it can be concluded that the assumption behind the model of infinitely high heat transfer is well justified for the small 2-mm particle size and has only a minor contribution to the outcome. This has also been shown in Fig. 10 in section 4.1.3. It must be noted that only a slight increase in particle diameter would lead to significant deviations from the CS model.

5. Summary and conclusion

With the present work an extensive parametric study on packed bed models for molten salt thermocline filler thermal energy storage systems was carried out. To cover a realistic parameter range, four storage configurations suitable for a 100 MW_{el} solar thermal power plant were considered. Two thermal energy storages were designed for 6 h storage capacity and two for 12 h, respectively. For each capacity either a mono-sized 2-mm packing or a bidisperse packing with 2- and 50-mm basalt rocks was considered. Models compared were the Schumann, single-phase and a recently developed bidisperse model. Additionally, the impact of effective conductivity of the bed was investigated by the utilization of the continuous-solid-phase model as well as wall losses and variable fluid properties were considered. As boundary conditions different use cases, namely the single blow and cyclic operation as well as annual simulations were considered. Results are qualitatively condensed in Table 11 and can be summarized with conclusions as follows:

- **Preliminary investigations** showed that the selection of a suitable model should be carried out carefully. For the single-phase model, cycling duration differed up to 25% from the reference model when a bidisperse packing with large particles was simulated. Contrary, the specifically designed bidisperse model showed no advantage for small sized particle packings. It was also shown that simulations with small particles are demanding due to strong temperature gradients and they require a very fine spatial and temporal resolution of the computing grid.
- The **single-phase model** showed similar results as the continuous-solid-phase model for small mono-sized packings in all use cases. The size of the storage volume, however, had little impact on the model outcome. It can be concluded that the single-phase model is suitable as long as the assumption of equal temperature of solid and fluid is justified, which is the case for small particles only.
- The **bidisperse model** becomes more accurate with increasing ratio of larger to smaller particles since both particle sizes are modeled individually. Larger particles dominate heat transfer resistance which is underestimated in models considering a mean diameter, such as the Schumann model. In comparison, the bidisperse model thus yielded approx. 2% less extracted exergy from the storage within the annual simulation. Since the more precise formulation of the bidisperse model mainly affects the convective term, the differences between the models further increased with longer operation times as in the storage size.
- In the single blow and cyclic operation studies, **effective conductivity** (continuous solid phase - CS model) showed generally a high impact with small particle packings as strong thermal gradients occur. Also, during stand-by conditions (hold phase) effective conductivity should always be considered. Only with comparatively large particles and high convective influence it can be neglected. These findings were also supported by the annual simulations, where significantly high differences >2.5% in exergy output occurred only with small particle packings and a large storage configuration with low flow velocity.
- **Wall losses** expectedly scale with outer surface area compared to the volume. During the 24 h stand-by periods (hold phase), the temperatures at the top and bottom nodes significantly dropped >30 Kelvin. This is caused by the comparatively large surface areas associated with these nodes. For the annual simulations, the difference in exergy output between the CS models with and without wall loss is just 0.5 percentage points for the 12 h storage configurations. Therefore, heat losses should be carefully evaluated depending of the use case. While the influence of storage size was evident, the influence of particle size, however, was low. In absolute numbers wall losses play only a minor role and their neglection is usually well justified.

- **Variable fluid properties** had a visible impact on the single blow operation and the duration of the charging and discharging periods of the cyclic operation. In those cases, the charging was faster than the discharging (up to ~0.5%). This can be explained by asymmetric variations in the temperature profiles which eventually lead to an asymmetric progression of the thermal power between charging and discharging periods. In the perspective of longer time frames, however, the differences average out. As a result, annual simulations showed just a maximum of 0.2% difference in exergy output.

As a general rule of thumb, we can derive the following recommendation: If the desired accuracy is better than 2%, the single-phase model should be avoided if particles >10 mm are present, while the bidisperse model gets advantageous the size ratio between small and large particles is >10. Effective conductivity is necessary only if stand-by periods are dominating or packings with particles smaller than 10 mm are present. Finally, we observed that heat losses and variable fluid properties appear neglectable for typical molten salt based thermal energy storage systems when applied to long duration use cases (cyclic and annual simulation). Thus, we recommend to use also a full charge and discharge cycle with a stand-by period in between for model validation.

For a future publication we recommend an investigation of different heat transfer correlations on the outcome of long-duration simulations.

Declaration of Competing Interest

The authors declare that they have no known competing financial interests or personal relationships that could have appeared to influence the work reported in this paper.

The authors have personal relationships with other researchers within the German Aerospace Center.

Data availability

The authors do not have permission to share data.

Acknowledgements

The authors thank the German Federal Ministry for Economic Affairs and Climate Action (BMWK) for the financial support given for this work in the project TransTES-Chem (Contract No. 03ET1646).

References

[1] D. Kunii, J.M. Smith, Heat transfer characteristics of porous rocks, AICHE J. 6 (1) (Mar. 1960) 71–78, https://doi.org/10.1002/aic.690060115.
[2] A.R. Balakrishnan, D.C.T. Pei, Heat transfer in gas-solid packed bed systems. 1. A critical review, Indust. Eng. Chem. Process Des. Develop. 18 (1) (Jan. 1979) 30–40, https://doi.org/10.1021/i260069a003.
[3] J.S. Wieringen, Exact and approximate solution of the regenerator equation for the case of high heat exchange and moderate heat capacity, Appl. Sci. Res. 34 (2–3) (1978) 145–158, https://doi.org/10.1007/BF00418863.
[4] D.E. Beasley, J.A. Clark, Transient response of a packed bed for thermal energy storage, Int. J. Heat Mass Transf. 27 (9) (1984) 1659–1669.
[5] A. Meier, C. Winkler, D. Wuillemin, Experiment for modelling high temperature rock bed storage, Solar Energy Mater. 24 (1991) 255–264, https://doi.org/10.1016/0165-1633(91)90066-T.
[6] T.M. Sanderson, G.T. Cunningham, Performance and efficient design of packed bed thermal storage systems. Part 1, Appl. Energy 50 (2) (Jan. 1995) 119–132, https://doi.org/10.1016/0306-2619(95)92628-7.
[7] F.W. Schmidt, A.J. Willmott, Thermal Energy Storage and Regeneration, 1st ed., Hemisphere Publishing Corporation, Washington, D.C., USA, 1981.
[8] A. Willmott, Dynamics of Regenerative Heat Transfer, 1st ed., Taylor & Francis, London, 2002.
[9] K.A.R. Ismail, R. Stuginsky Jr., A parametric study on possible fixed bed models for pcm and sensible heat storage, Appl. Therm. Eng. 19 (7) (1999) 757–788, https://doi.org/10.1016/S1359-4311(98)00081-7.
[10] A. Elouali, et al., Physical models for packed bed: sensible heat storage systems, Journal of Energy Storage 23 (Jun. 2019) 69–78, https://doi.org/10.1016/j.est.2019.03.004.
[11] T. Esence, A. Bruch, S. Molina, B. Stutz, J.F. Fourmigué, A review on experience feedback and numerical modeling of packed-bed thermal energy storage systems, Sol. Energy 153 (2017) 628–654, https://doi.org/10.1016/j.solener.2017.03.032.
[12] I. Calderón-Vásquez, et al., Review on modeling approaches for packed-bed thermal storage systems, Renew. Sust. Energ. Rev. 143 (Jun. 2021), 110902, https://doi.org/10.1016/j.rser.2021.110902.
[13] J.E. Pacheco, Final Test and Evaluation Results from the Solar Two Project, 2002, https://doi.org/10.2172/793226.
[14] A. Mawire, M. McPherson, Experimental and simulated temperature distribution of an oil-pebble bed thermal energy storage system with a variable heat source, Appl. Therm. Eng. 29 (5–6) (2009) 1086–1095, https://doi.org/10.1016/j.applthermaleng.2008.05.028.
[15] C.S. Libby, Solar Thermocline Storage Systems: Preliminary Design Study, EPRI, 2010. Report no. 1019581, EPRI, California.
[16] B. Zhao, M. Cheng, C. Liu, Z. Dai, An efficient tank size estimation strategy for packed-bed thermocline thermal energy storage systems for concentrated solar power, Sol. Energy 153 (Sep. 2017) 104–114, https://doi.org/10.1016/j.solener.2017.05.057.
[17] Z. Yang, S.V. Garimella, Cyclic operation of molten-salt thermal energy storage in thermoclines for solar power plants, Appl. Energy 103 (2013) 256–265, https://doi.org/10.1016/j.apenergy.2012.09.043.
[18] Z. Yang, S.V. Garimella, Thermal analysis of solar thermal energy storage in a molten-salt thermocline, Sol. Energy 84 (6) (Jun. 2010) 974–985, https://doi.org/10.1016/j.solener.2010.03.007.
[19] S.M. Flueckiger, Z. Yang, S.V. Garimella, Review of molten-salt thermocline tank modeling for solar thermal energy storage, Heat Transfer Eng. 34 (10) (Aug. 2013) 787–800, https://doi.org/10.1080/01457632.2012.746152.
[20] J.-F. Hoffmann, T. Fasquelle, V. Goetz, X. Py, A thermocline thermal energy storage system with filler materials for concentrated solar power plants: experimental data and numerical model sensitivity to different experimental tank scales, Appl. Therm. Eng. 100 (2016) 753–761, https://doi.org/10.1016/j.applthermaleng.2016.01.110.
[21] M.M. Valmiki, W. Karaki, P. Li, J.V. Lew, C. Chan, J. Stephens, Experimental investigation of thermal storage processes in a thermocline tank, J. Solar Energy Eng. 134 (4) (2012), 041003, https://doi.org/10.1115/1.4006962.
[22] J.T. Van Lew, P. Li, C.L. Chan, W. Karaki, J. Stephens, Transient Heat Delivery and Storage Process in a Thermocline Heat Storage System, Jan. 2009, pp. 139–148, https://doi.org/10.1115/IMECE2009-11701.
[23] P. Li, J. Van Lew, W. Karaki, C. Chan, J. Stephens, Q. Wang, Generalized charts of energy storage effectiveness for thermocline heat storage tank design and calibration, Sol. Energy 85 (9) (Sep. 2011) 2130–2143, https://doi.org/10.1016/j.solener.2011.05.022.
[24] K.S. Reddy, V. Jawahar, S. Sivakumar, T.K. Mallick, Performance investigation of single-tank thermocline storage systems for CSP plants, Sol. Energy 144 (Mar. 2017) 740–749, https://doi.org/10.1016/j.solener.2017.02.012.
[25] P.A. Galione, C.D. Pérez-Segarra, I. Rodríguez, S. Torras, J. Rigola, Multi-layered solid-PCM thermocline thermal storage for CSP. Numerical evaluation of its application in a 50MWe plant, Sol. Energy 119 (Sep. 2015) 134–150, https://doi.org/10.1016/j.solener.2015.06.029.
[26] E.V. Votyakov, A.M. Bonanos, A perturbation model for stratified thermal energy storage tanks, Int. J. Heat Mass Transf. 75 (2014) 218–223, https://doi.org/10.1016/j.ijheatmasstransfer.2014.03.071.
[27] A.M. Bonanos, E.V. Votyakov, Sensitivity analysis for thermocline thermal storage tank design, Renew. Energy 99 (2016) 764–771, https://doi.org/10.1016/j.renene.2016.07.052.
[28] R. Bayón, E. Rojas, Simulation of thermocline storage for solar thermal power plants: from dimensionless results to prototypes and real-size tanks, Int. J. Heat Mass Transf. 60 (1) (2013) 713–721, https://doi.org/10.1016/j.ijheatmasstransfer.2013.01.047.
[29] H. Yin, J. Ding, R. Jiang, X. Yang, Thermocline characteristics of molten-salt thermal energy storage in porous packed-bed tank, Appl. Therm. Eng. 110 (Jan. 2017) 855–863, https://doi.org/10.1016/j.applthermaleng.2016.08.214.
[30] S.M. Flueckiger, B.D. Iverson, S.V. Garimella, J.E. Pacheco, System-level simulation of a solar power tower plant with thermocline thermal energy storage, Appl. Energy 113 (Jan. 2014) 86–96, https://doi.org/10.1016/j.apenergy.2013.07.004.
[31] X. Yang, X. Yang, J. Ding, Y. Shao, F.G.F. Qin, R. Jiang, Criteria for performance improvement of a molten salt thermocline storage system, Appl. Therm. Eng. 48 (Dec. 2012) 24–31, https://doi.org/10.1016/j.applthermaleng.2012.04.046.
[32] C. Xu, Z. Wang, Y. He, X. Li, F. Bai, Sensitivity analysis of the numerical study on the thermal performance of a packed-bed molten salt thermocline thermal storage system, Appl. Energy 92 (Apr. 2012) 65–75, https://doi.org/10.1016/j.apenergy.2011.11.002.
[33] C. Xu, X. Li, Z. Wang, Y. He, F. Bai, Effects of solid particle properties on the thermal performance of a packed-bed molten-salt thermocline thermal storage system, Appl. Therm. Eng. 57 (1–2) (Aug. 2013) 69–80, https://doi.org/10.1016/j.applthermaleng.2013.03.052.
[34] K. Niedermeier, L. Marocco, J. Flesch, G. Mohan, J. Coventry, T. Wetzel, Performance of molten sodium vs. molten salts in a packed bed thermal energy storage, Appl. Therm. Eng. 141 (Aug. 2018) 368–377, https://doi.org/10.1016/j.applthermaleng.2018.05.080.
[35] B. Kocak, H.O. Paksoy, Numerical model of lab-scale packed-bed thermal energy storage system, in: *Proceedings of the 13th International Renewable Energy Storage Conference* 2019 *(IRES 2019)*, Düsseldorf, Germany, 2019, https://doi.org/10.2991/ires-19.2019.7.

[36] C. Odenthal, F. Klasing, T. Bauer, A three-equation thermocline thermal energy storage model for bidisperse packed beds, Sol. Energy 191 (Oct. 2019) 410–419, https://doi.org/10.1016/j.solener.2019.09.005.
[37] F.W. Schmidt, A.J. Willmott, Thermal Energy Storage and Regeneration, 1st ed., Hemisphere Publishing Corporation, Washington, D.C., USA, 1981.
[38] T.E.W. Schumann, Heat transfer: a liquid flowing through a porous prism, Journal of the Franklin Institute 208 (3) (Sep. 1929) 405–416, https://doi.org/10.1016/S0016-0032(29)91186-8.
[39] N. Wakao, S. Kagei, Heat and Mass Transfer in Packed Beds, Gordon and Breach Science Publishers Inc., New York, 1982.
[40] R.G. Deissler, J.S. Boegli, An investigation of effective thermal conductivities of powders in various gases, Trans. Am. Soc. Mech. Eng. 80 (1958).
[41] T. Bauer, N. Pfleger, N. Breidenbach, M. Eck, D. Laing, S. Kaesche, Material aspects of solar salt for sensible heat storage, Appl. Energy 111 (2013) 1114–1119.
[42] P. Hartlieb, M. Toifl, F. Kuchar, R. Meisels, T. Antretter, Thermo-physical properties of selected hard rocks and their relation to microwave-assisted comminution, Miner. Eng. 91 (May 2016) 34–41, https://doi.org/10.1016/j.mineng.2015.11.008.
[43] F. Klasing, T. Hirsch, C. Odenthal, T. Bauer, Techno-economic optimization of molten salt concentrating solar power parabolic trough plants with packed-bed thermocline tanks, J. Solar Energy Eng. 142 (5) (Oct. 2020), 051006, https://doi.org/10.1115/1.4046463.
[44] V. Quaschning, W. Ortmanns, R. Kistner, M. Geyer, greenius - A New Simulation Environment for Technical and Economical Analysis of Renewable Independent Power Projects, 2001, p. 5.
[45] S.E. Faas, L.R. Thorne, E.A. Fuchs, N.D. Gilbertsen, 10 MWe Solar Thermal Central Receiver Pilot Plant: Thermal Storage Subsystem Evaluation Final Report, 1986.
[46] M.J. Rhodes, Introduction to Particle Technology, 2nd ed., Wiley, Chichester, England ; Hoboken, NJ, 2008.
[47] E. González-Roubaud, D. Pérez-Osorio, C. Prieto, Review of commercial thermal energy storage in concentrated solar power plants: steam vs. molten salts, Renew. Sust. Energ. Rev. 80 (Dec. 2017) 133–148, https://doi.org/10.1016/j.rser.2017.05.084.